This dissertation has been
microfilmed exactly as received

69-18,012

GORDON, Kurtiss Jay, 1940-
A 21-CM STUDY OF THE SPIRAL GALAXY MESSIER 33.

The University of Michigan, Ph.D., 1969
Astronomy

University Microfilms, Inc., Ann Arbor, Michigan

A 21-CM STUDY OF

THE SPIRAL GALAXY MESSIER 33

by

Kurtiss Jay Gordon

A dissertation submitted in partial fulfillment
of the requirements for the degree of
Doctor of Philosophy in
The University of Michigan
1969

Doctoral Committee:

Professor Freeman D. Miller, Chairman
Professor David M. Dennison
Professor Fred T. Haddock
Doctor Morton S. Roberts, National Radio Astronomy Observatory
Assistant Professor Peter A. Wehinger

ABSTRACT

A 21-CM STUDY OF THE SPIRAL GALAXY MESSIER 33

by

Kurtiss Jay Gordon

Chairman: Freeman D. Miller

The distribution of neutral atomic hydrogen and the kinematic properties of the late-type spiral galaxy M33 are derived from observations obtained at 21-cm wavelength with a multichannel radiometer attached to the 300-foot paraboloidal transit telescope of the National Radio Astronomy Observatory. The effective half-power beam and band widths of the telescope system are 10!0 in δ, 11!4 in α, and 21 km/sec in radial velocity. The assumed distance to M33 is 720 kpc. The galaxy contains M_{HI} = 1.6×10^9 $M_\odot$ of neutral hydrogen distributed in a broad ring of radius 18' plus an underlying uniform distribution of radius $\sim$35' and two outlying "wings" or companions. The companions contain $\sim$10% of the total hydrogen content. The center of the H I ring and of the distributions of H II regions and luminous stars in M33 are offset by a few minutes of arc from the optical center of the galaxy.

The systemic radial velocity is S = -180 km/sec (heliocentric). The rotation curve peaks at $V_r = S \pm \sim 85$ km/sec, 30' from the galactic center. For an inclination of 55^c, this leads to a total mass of $M_t = 4.9 \times 10^{10}$ $M_\odot$, of which 2.3×10^{10} $M_\odot$ is contained within 60' of the center (roughly the extent of the observations). An asymmetry of the rotation curves for the two halves of the major axis leads to a mass ratio of $M_N/M_S = 1.2$. Noncircular motions are small in the main body of the galaxy. Velocities in the wings deviate by 40-50 km/sec from those predicted by the rotation curve. The data are consistent with a picture of the wings

as stable gaseous companions of M33, gravitationally bound to the galaxy but not physically connected to the galactic plane. The global parameters of M33: $M_{HI}/M_t = 0.03$, $M_{HI}/L_O = 0.34$, and $M_t/L_O = 10.4$ (solar units), are not significantly different from average values of the corresponding parameters for galaxies of similar structural type.

A search for a bridge of neutral hydrogen between M31 and M33 yields an upper limit of $N_{HI} \leq 5 \times 10^{14}$ cm^{-2} in the region between the galaxies. This limit is roughly 1/4 of the observed surface density in the bridge between NGC 4631 and NGC 4656 and 1/6 of the observed density in the bridge between the Magellanic Clouds. The model-fitting technique described and used in this study has been shown to be a powerful tool for studying the kinematics and hydrogen distribution of galaxies.

ACKNOWLEDGMENTS

It is a pleasure to thank Dr. M. S. Roberts for his constant help and guidance throughout all stages of my thesis. Many of the data analyzed herein were originally obtained by him and generously placed at my disposal. Special thanks must also go to Dr. F. D. Miller, the chairman of my committee. He has offered many perceptive and constructive suggestions and has cheerfully endured the added inconvenience of advising his student via mail. Appreciation is expressed to Dr. D. M. Dennison, Prof. F. T. Haddock, and Dr. P. A. Wehinger for their thoughtful readings of my thesis.

Several authors have very kindly allowed me to use their data in advance of publication. I have received Hα interferometric velocities from Dr. G. Courtès, star counts from Dr. G. de Vaucouleurs, Dr. J. L. Sérsic's catalog of Hα emission regions from Dr. A. R. Sandage, unpublished data on emission regions from Dr. L. H. Aller, and a value for the hydrogen mass of M33 from Mr. S. Y. Meng. I am also grateful for the opportunity to discuss the comparisons of the optical and radio observations with Dr. Courtès, Dr. de Vaucouleurs, and Dr. Aller.

The preparation of the thesis was greatly facilitated by the aid of the excellent supporting staff of the National Radio Astronomy Observatory*. Its content has benefited markedly from many helpful discussions with and comments from my wife Courtney; and its completion is due in no small part to her constant encouragement.

* Operated by Associated Universities, Inc., under contract with the National Science Foundation.

TABLE OF CONTENTS

page

ACKNOWLEDGMENTS ii

LIST OF TABLES v

LIST OF FIGURES vi

Chapter

I. BACKGROUND 1

1. Introduction
2. History
   a) The Island Universe Theory
   b) Modern Studies of M33
      (1) Photometry
      (2) Morphology
      (3) Emission Nebulae
      (4) Radio Continuum
      (5) Neutral Hydrogen
      (6) Stellar Content
      (7) Kinematics

II. OBSERVATIONS 17

III. NEUTRAL HYDROGEN DISTRIBUTION 21

1. Mass
2. Form of the Distribution
3. Comparison with the Distributions of Other Galactic Constituents
   a) Star Counts
   b) B Photometry
   c) Ionized Hydrogen
   d) Discussion
4. Search for a Neutral-Atomic-Hydrogen Link Between M31 and M33

IV. KINEMATICS 42

1. General Considerations and Assumptions
2. The Model-Fitting Program
   a) Coordinate Systems
   b) Parameters of the Model Galaxy
   c) Parameters of the Receiving System
   d) The Channel Receptivity Field
   e) The Antenna Temperature
   f) The Numerical Integration Algorithm
   g) Comparison with Observed Data

Chapter Page

3. The Observations and the Models
   a) Observational Data
   b) Hydrogen Distribution
   c) Inclination
   d) Systemic Velocity
   e) The Rotation Curve and the Total Mass of M33
   f) Comparison of the Distributions of Mass, Light, and Neutral Hydrogen
   g) Departures from Circular Motion
   h) Comparison of the Kinematics of Neutral and Ionized Hydrogen
   i) Kinematics of the Outermost Parts of the Galaxy

V. SUMMARY 83

BIBLIOGRAPHY 88

LIST OF TABLES

Table		page
1.	Number of Observations Obtained at Various Declinations . . .	20
2.	Observed Diameters and Offsets of M33 Constituent Distributions	32
3.	Comparison of Intergalactic H I Bridges	41
4.	Peaks of Single-Channel Contour Maps	58
5.	Adopted Values for H I Distribution Parameters	60
6.	Determinations of the Inclination of M33	61
7.	The Systemic Velocity of M33	62
8.	Parameters of the Rotation Curve	65
9.	The Total Mass of M33	67
10.	Comparison of the Distributions of Mass, Light, and Neutral Hydrogen	69
11.	Model Fitting for Velocity Profiles off the Major Axis . . .	70
12.	Model Fitting for Velocity Profiles in the Wings	77
13.	Summary of the Properties of Messier 33	84

LIST OF FIGURES

Figure		Page
1.	The Earl of Rosse's Drawing and Description of Messier 33 . .	4
2.	The Radio Continuum Spectrum	12
3.	Integrated 21-cm Brightness Distribution	22
4.	Cross Sections of Individual-Channel Brightness Distributions	24
5.	Distribution of Stars Brighter than $m_{pg} = 20.2$	26
6.	B Photometry	28
7.	Distribution of Hα Emission Regions	30
8.	Comparison of the Constituent Distributions	33
9.	Local Group Projected into the Supergalactic Plane	36
10.	Drift Scans through M31 and M33	38
11.	Velocity Profile of the Intergalactic Region	40
12.	Coordinate Systems Used in the Model-Fitting Program	45
13.	A Model Galaxy in Pure Rotation	50
14.	Individual-Channel Contour Maps	54
15.	Model-Galaxy Contour Maps	59
16.	Radial-Velocity Loci (Peaks)	73
17.	Radial-Velocity Loci (Midpoints)	74
18.	Radial Velocity Range	76

CHAPTER I: BACKGROUND

1. Introduction

Messier 33 (= NGC 598) in the constellation Triangulum has the largest angular size of any late-type spiral galaxy. Only three other extragalactic objects, the Magellanic Clouds and Messier 31 in Andromeda, exceed the apparent dimensions of M33. And only M31 is also visible from the northern hemisphere. The large size and favorable inclination of M33 make it an excellent object for study. Our own galaxy, the Milky Way, has traditionally been compared to the Andromeda galaxy. However, several recent observational results indicate that the Milky Way may be later in morphological type than M31. Hence the best model for our galaxy may turn out to be a judicious interpolation between models obtained for M31 and M33.

The observations used in this study are of the 21-cm spectral line of neutral atomic hydrogen, caused by a transition between two hyperfine levels in the ground state of the atom. They were obtained with a multi-channel radiometer attached to the 300-foot meridian transit reflector of the National Radio Astronomy Observatory in Green Bank, W. Va. The equipment and observational techniques are described in Chapter II. The data from these observations provide information on the spatial distribution of neutral atomic hydrogen in the galaxy. The distribution may be compared with the distributions of other constituents of the galaxy, obtained by other investigators in previous studies. These results are described in Chapter III.

The frequency resolution of the receiver yields Doppler-shift measurements of the component of motion of the neutral hydrogen in the line of

sight. With the aid of these measurements and some assumptions regarding the possible types of motions in the galaxy, we describe in Chapter IV the kinematic properties of the neutral hydrogen in M33. By considering these atoms as test particles in the gravitational field of the galaxy, we draw conclusions about the galaxy's total mass and mass distribution. In the final chapter, we summarize the results of our study of M33 and relate them to findings for other galaxies of similar type.

2. History

a) The Island Universe Theory

The idea that our sun is just one of myriads of stars in a huge stellar system, the Milky Way, and that there may be many other stellar systems of equal rank outside the Milky Way can be traced back to the early 18th century (Lundmark 1927). These early speculations by the Swedish philosopher Emanuel Swedenborg and, independently, by Thomas Wright of Durham in England had no basis in actual observations. Yet they are remarkably close to the present day views of the cosmos. The best-known of the early exponents of the "island universe" theory are the German philosopher Immanuel Kant, who acknowledged his indebtedness to the ideas of Wright, and the English astronomer Sir William Herschel, who was the first to bring observational techniques to bear specifically on the study of nebulae and clusters of stars. In contrast, Messier compiled his catalog of nebulae and clusters, which predates Herschel's work, primarily as a list of "nuisances" to be avoided in his search for new comets (Gingerich 1960).

At first it was not possible observationally to distinguish between gaseous nebulae and stellar aggregations, and it was thought that all nebulae were groups of stars--some of them so distant that individual

stars could not be resolved. Herschel even attempted to estimate the distances to nebulae on the basis of the amount of incipient resolution into stars. Then he found the planetary nebula NGC 1514 which, from its appearance (see Curtis 1918, Pl. IX), was obviously a single star associated with faint nebulosity, a "nebulous star." Because of this, and from the fact that star counts in selected regions ("gauges") did not enable him to penetrate to the outside of the Milky Way, Herschel totally revised his thinking, now maintaining that all nebulae were small compared to the Milky Way and were encompassed within it. The controversy between the two views was not to be resolved for more than a century after his death in 1822.

The observations by the Earl of Rosse with his 72-inch reflector raised the fortunes of the island universe theory again. In 1845 he found the spiral nature of M51. His paper in 1850 contained drawings of five spiral nebulae, including M33 (see Fig. 1), and listed fourteen more. He also remarked that some of these spirals could be resolved into stars. On this basis, and using the star counts made by the Herschels, Alexander (1852) suggested "that the Milky Way and the stars within it together constitute a spiral with several (it may be four) branches," and traced the branches across the sky. But Herbert Spencer argued in his book, published in 1862, that since all stars are of similar sizes, all nebulae should be of similar sizes; and if the nebulae are actually stellar aggregations, then the apparently largest and presumably closest should be resolvable while the smallest and furthest should remain unresolved. In arguing that many quite small nebulae could in fact be resolved, Spencer mistook small clusters for nebulae. However, this was not immediately recognized.

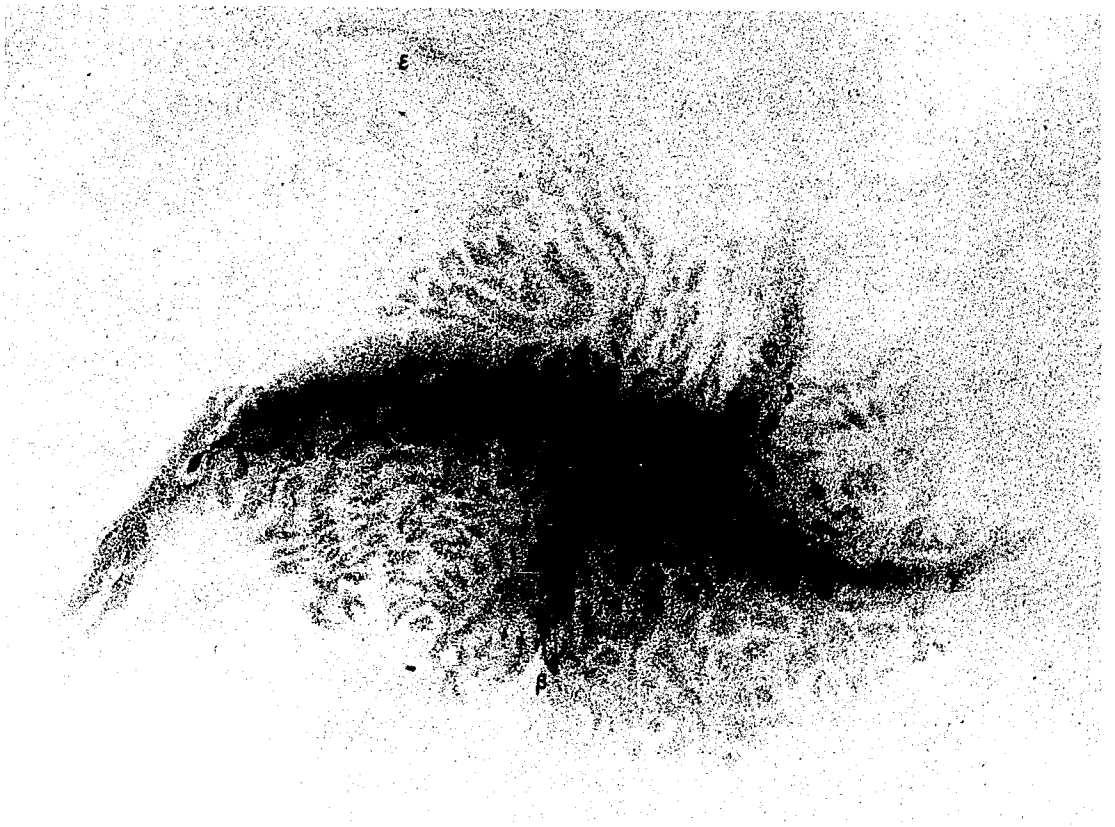


Plate XXXVI. fig. 5, H. 131 — This figure represents the central portion of a very large nebula. The nebula itself has not been sufficiently examined, but as yet no other portion appears to have a spiral, or indeed any regular arrangement. The sketch is not very accurate, but represents sufficiently well the general character of the central portion.

"September 6, 1849. — A spiral.

"September 16, 1849. — New spiral; α the brightest branch; γ faint; δ short but pretty bright; β pretty distinct; ε but suspected; the whole involved in faint nebula which probably extends past several knots which lie about it in different directions. Faint nebula seems to extend very far following: drawing taken.

"September 10, 1849. — An attempt at a drawing taken: fog.

"October 1849. — The whole nebula in flocculi."

Figure 1. — The Earl of Rosse's Drawing and Description of Messier 33 (from Rosse 1850).

In 1864, Sir William Huggins observed several nebulae with a spectroscope, finding first an emission-line spectrum for the planetary nebula NGC 6543 and, a few nights later, a continuous spectrum with a hint of absorption features for the great Andromeda nebula. This showed that nebulae could be divided into two fundamentally distinct classes: those that were clouds of luminous gas and those that were stellar aggregations. All of the spiral nebulae were found to belong to the latter class. The conclusive evidence of this was presented by Scheiner (1899) in the form of the first good-quality spectrogram of a spiral nebula, M31.

The application of photography to studies of nebulae made it possible to get more detailed pictures of the form of the spiral nebulae. The pioneering work in this field was done by the Irish amateur astronomer Isaac Roberts (Roberts 1893, 1899: M33 is in Plate 10 of the latter) and by J. E. Keeler with the 36-inch Crossley reflector of the Lick Observatory (Keeler 1908: M33 is in Plate 3). On the basis of these photographs, the spiral nebulae were subclassified into a "condensed" type, showing condensations or knots of incipient resolution over the entire face of the nebula, and an "uncondensed" type, showing incipient resolution only in the outermost parts of the nebula, if at all. The prototypes of the two groups were M33 and M31, respectively. Dreyer (1904), using photographs taken by Roberts, published a catalog of the condensations in M33 with the intent that it form a basis for determining whether there were any changes in the nebula in the course of time. Van der Pahlen (1911) attempted to fit the forms of the arms of spirals to mathematical curves. He found that the two main arms of M33 fit

logarithmic spirals quite well, but that they had different rates of coiling and that they were not 180° apart. Wolf and Ernst (1913) catalogued 517 knots of nebulosity in a region centered on M33, extending over a diameter of several degrees but omitting the portion within 25' of its nucleus. They found that the nebulae tended to concentrate in patterns which looked like extensions of the spiral arms so prominent in the inner part of M33. They claimed that the spiral pattern could be followed over a region 8° in diameter and concluded that M33 must therefore be quite nearby.

The following year Slipher (1914) reported a radial velocity of -300 km/sec for M31, and Wolf (1914) reported the first spectrographic measurements of internal motions of spirals, finding rotational velocities of 100 km/sec in M81. In a larger-scale survey of the motions of spirals, Slipher (1915) noted that their average velocity was roughly 25 times as large as the average stellar velocity, larger than for any other class of astronomical objects. He also found large internal motions, evidenced by a rotational velocity of the edge-on spiral NGC 4594 of 100 km/sec 20" from the nucleus. Pease (1915, 1916) confirmed the finding of large internal motions in spirals by measuring a difference of roughly 200 km/sec between the radial velocities of the nucleus of M33 and of NGC 604, a bright condensation 10' from the nucleus. The large systemic radial velocities indicated that the spirals could not be gravitationally bound by the Milky Way, and were thus at least not permanent members of it. The radial-velocity measurements of internal motions, if they could be combined with proper-motion data, would provide a direct measurement of the distances of the spirals.

During the first few years the Mt. Wilson 60-inch telescope was in operation, Ritchey had obtained the best nebular photographs yet. His pictures of the condensed type of spirals showed many points in the nebulae which could be measured for proper motion. Second epoch plates were taken and measured by van Maanen. In 1916 he reported finding motions in M101 which could be interpreted either as rotation or as outward streaming along the spiral arms. In either case, the fact that proper motions could be measured in the spirals indicated that they were nearby objects. His paper on M33 (1923) contains a summary of his measurements and interpretations. To provide a check on these critical measurements, Lundmark independently remeasured the more than 400 points on van Maanen's plates of M33. Although his results correlated well with van Maanen's with respect to both direction and relative size of proper motion, the absolute scale of Lundmark's proper motions was less than 1/10 as large as those van Maanen had measured (Lundmark 1926).

Meanwhile, evidence supporting the extragalactic interpretation of spiral nebulae began to mount up. Spurred by the first photographic discovery of a nova in a spiral nebula (Ritchey, reported by Pickering 1917), Ritchey (1917) and Curtis (1917) examined the large plate collections of Mt. Wilson and Lick Observatories and found a score of others that had gone undetected in previous years, including two in M31. Systematic surveys over the next two years produced 14 additional novae in M31, but none in any other spiral. These formed a homogeneous group, all peaking at about $m_{pg} = 17$, about 10 magnitudes fainter than the visually detected nova S Andromedae of 1885 in M31. S And, on the other hand, was the only nova in M31 which conformed to the pattern of the novae discovered in other spirals, all of which had light outputs which

were appreciable fractions of the total light outputs of the associated nebulae. At this time there was no compelling reason to choose either type of nova to represent the analog of the galactic novae.

In 1921, Lundmark found that counts of stars brighter than m_{pg} = 15.7 in the field of M33 were not influenced by the presence of the nebula. Hence M33 had to be further away than the average $15^{m}.7$ star, roughly 3 kpc. Moreover, if the brightest stars in M33 had absolute magnitudes of -6, it had to be 300 kpc away. In 1922, Duncan discovered three recurrent variable stars in M33, the first found in any spiral. He also reported a suspected nova. By the end of 1924, Hubble (1925) had assembled data on 47 variables in M33, 22 of which were Cepheids obeying the same period-color index and period-amplitude relations as the Cepheids in the Milky Way and the Magellanic Clouds. Applying the period-luminosity law, Hubble derived a distance of 285 kpc to M33, and a comparable result from similar data for M31. These distances agreed with those derived from the brightest nonvariable stars and with those derived by choosing to identify the fainter of the two types of novae in M31 with galactic novae. Star counts in M33 (Hubble 1926), coupled with the Cepheid distance scale, showed that its luminosity function agreed with Kapteyn's luminosity function for the Milky Way, and thus appeared to settle the island-universe controversy. The one remaining loose end was the question of the reality of van Maanen's rotations. This was decided negatively on the basis of plates of M33 and M74 from the Mt. Wilson 100-inch telescope (Hubble 1935, van Maanen 1935).

b) Modern Studies of M33

(1) Photometry. — Whitford (1936) measured M33 photoelectrically through a 54' circular diaphragm, and obtained m_{pg} = 6.9 after correction

for foreground stars and conversion to the international scale. Stebbins and Whitford (1937, 1948, 1952) included M33 in their photoelectric photometry of galaxies. In all three studies they used diaphragms of fixed sizes, centered on the nucleus; none of the diaphragms was large enough to include more than a small central portion of M33. Tifft's (1961) four-color photometry and McClure's and van den Bergh's (1968) five-color photometry also included only the nuclear region of M33. Seyfert (1940) found that the spiral arms were barely visible on NS and EW tracings of photographs of M33 in red and blue light. The arms were somewhat bluer than the nucleus. Patterson (1940) discovered that the gradient of photographic luminosity followed an exponential law--photographic magnitude a linear function of radius--except within 6' of the nucleus. From microphotometer tracings every 30° of position angle, she found a position angle of the major axis of 20°, an inclination of the galactic plane of 60°, and an integrated m_{pg} of 6.0 out to 30'. Danver's (1942) results for position angle and inclination disagreed with those of Patterson and of more recent studies. However, he also noted the difference in pitch angle of the two main spiral arms (cf. van der Pahlen 1911), and he found that isophotes crossed the north-preceding half of the minor axis further away from the galactic nucleus than they crossed the south-following half. Currently, the definitive photometric studies of M33 are the photographic photometry by Holmberg (1950, 1952, 1958) on the international system and the photoelectric photometry by de Vaucouleurs (1959) on the UBV system. Voshakidze (1955) measured 13% mean optical polarization for M33, which was in line with the trend he found of percentage polarization increasing with advancing morphological type in a sample of 11 galaxies.

(2) Morphology. — The morphological type of M33 has been classified on all the existing systems: Sc (Hubble 1936), Sc^+ (Holmberg 1958), Sc II-III (van den Bergh 1960), SA(s)cd (de Vaucouleurs 1961a), fS3 or fS4 (Morgan 1958, 1959), and L; 22cd, Ha (Vorontsov-Velyaminov and Arkhipova 1964). Vorontsov-Velyaminov (1956a) noted that the spiral arms could be traced to within 75 pc (20") of the nucleus.

(3) Emission Nebulae. — The existence of emission nebulae within M33 has been known at least since Pease (1915) obtained a spectrogram of NGC 604. Detection of these emission regions has been accomplished primarily by comparison of blue plates (sensitive to [O II] 3727 Å) and/or red plates (sensitive to Hα) to yellow plates and/or infrared plates. Catalogs of emission regions have been compiled by Haro (1950), Aller (1954, 1956), Shajn (1954), and Sĕrsic (1959a). By means of narrow Hα interference filters Courtès and Cruvellier (1961, 1965) found many emission regions in the central portion of M33, which is burned out on plates obtained by more classical methods. Within the errors of measurement, the H II regions in M33 have the same chemical composition as those in our own galaxy (Mathis 1962; Aller, Czyzak, and Walker 1968), and the Magellanic Clouds (Aller and Faulkner 1962). Most of the emission nebulae are of low excitation (Mayall and Aller 1939), but some higher-excitation regions are found further from the nucleus (Aller 1942b). The linear diameters of the largest H II regions are quite similar to those in the LMC. They have been used as calibrators for a method of distance determination to the more distant galaxies (Sĕrsic 1959b, 1960; Sandage 1962; Tammann and Sandage 1968). The masses of the largest H II regions have been calculated by Shajn and Haze (1952, 1953). Their measurements yield, after conversion to the presently accepted distance scale, a mass of the

order of $3 \times 10^6 M_\odot$ for NGC 604, the largest H II region in M33. (All distance-dependent quantities have been recalculated for consistency with a distance of 720 kpc; Sandage 1962.)

In addition to the emission lines in the H II regions, a diffuse background of line emission has been found at 3727 Å (Mayall 1939) and at Hα and [N II] (Carranza, Courtès, Georgelin, Monnet, and Pourcelot 1968). The ratio of [N II] to Hα indicates higher excitation for this diffuse component than for the classical H II regions.

(4) Radio Continuum. — Continuum radiation from M33 at radio frequencies has been observed by Brown and Hazard (1959, 1961), Leslie (1960), Heeschen (1961), Venugopal (1963), Heeschen and Wade (1964), Kuril'chik and Sytsko (1965), and DeJong (1965, 1967). These measurements were made between 159 MHz and 3 GHz. The integrated flux densities can be represented approximately by a power-law spectrum, with $S(1\ \mathrm{GHz}) \approx 5$ flux units and $\alpha = -1.0$ (see Fig. 2). The 4C catalog (Pilkington and Scott 1965) contains no source within 45' of the position of the galaxy.

(5) Neutral Hydrogen. — The neutral hydrogen distribution was found to extend "far beyond the structure visible on the available photographs" (Dieter 1957) even in the earliest 21-cm line observations of M33. The angular resolution of these data was, however, insufficient to provide any details of the distribution. Davies and Burke (discussion following Burke, Turner, and Tuve 1964b) noted that their observations with the 250-foot and 300-foot telescopes, respectively, indicated a ring-shaped distribution of the neutral hydrogen in M33. The radius of this ring has been placed between 15' and 20' (Burke et al. 1964b; Meng and Kraus 1966; Roberts 1967). However, the center of the ring is

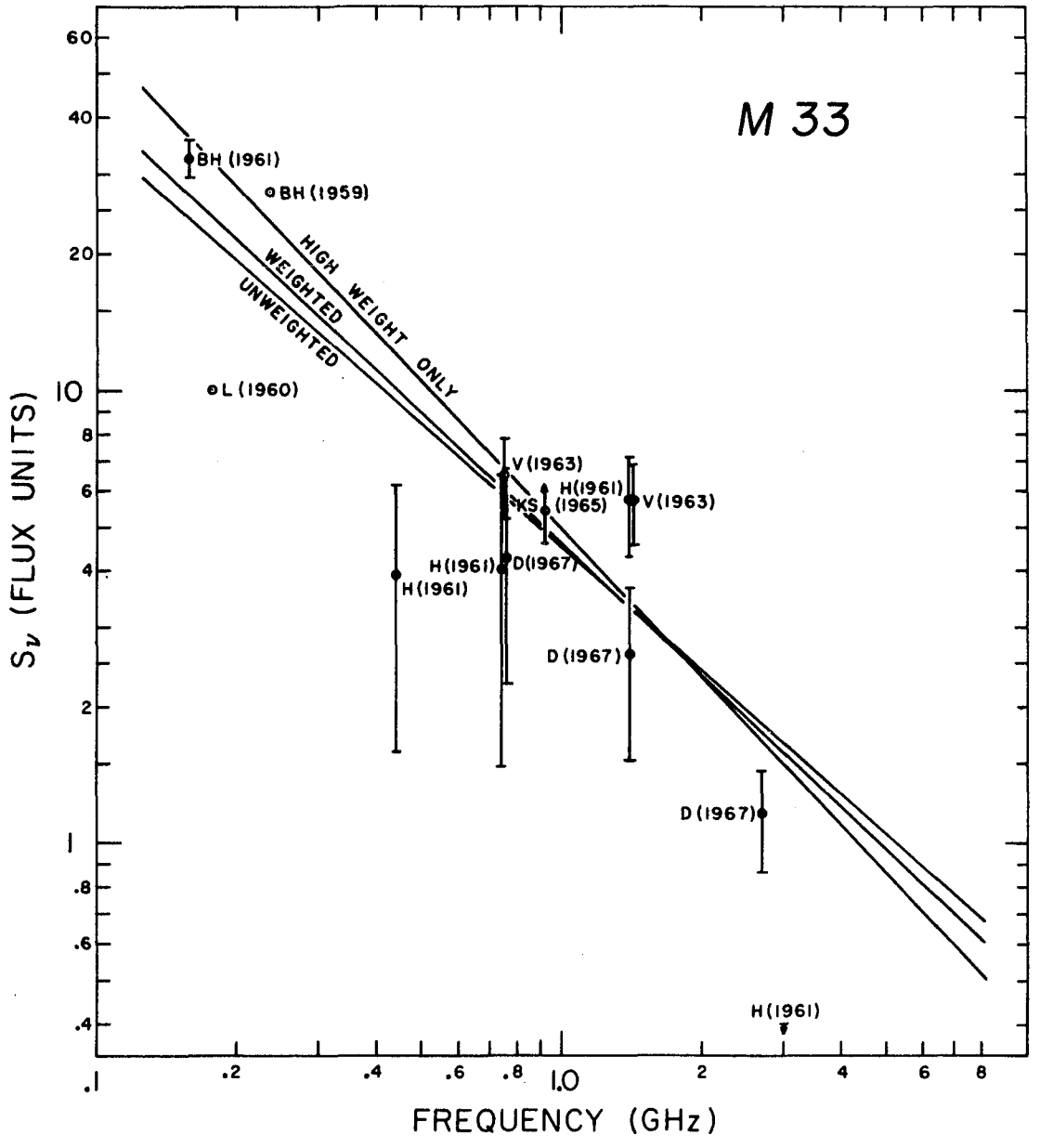


Figure 2. — The Radio Continuum Spectrum. The points are published integrated flux densities of M33, with mean errors indicated where known. The points are labeled with authors' initials and dates of publication (see the text for complete references). The lines represent three different linear least squares regression curves of log S_ν upon log ν. All points were used in the "weighted" and "unweighted" solutions. In the "weighted" solution, the four values obtained by mapping the galaxy (BH at 159 MHz, V at 750 and 1410 MHz, and D at 2795 MHz) were given double weight. Only these four points were used in the "high weight only" solution. (1 flux unit = 10^{-26} W m^{-2} Hz^{-1})

displaced by a few minutes of arc from the optical center of the galaxy (Gordon 1968), and there are other departures from axial symmetry.

(6) Stellar Content. — The first individual stars recognized in M33 were Duncan's (1922) three variables and a nova. Hubble (1925, 1926) --who at the time was interested primarily in determining the distance to M33--discussed this nova, Cepheids, and a luminosity function derived from star counts of selected fields within M33. De Vaucouleurs (1961b) extended the star counts to cover the entire face of M33 down to 20th photographic magnitude. On the basis of these counts, he found (de Vaucouleurs 1968) the center of the distribution of Population I stars to be displaced to the southwest of the optical center. Hubble and Sandage (1953) found that the brightest variable stars (intermediate-type supergiants) formed a group with a small dispersion in luminosity, thus providing another distance criterion for galaxies. Johnson and Sandage (reported by Johnson, Hoag, Iriarte, Mitchell, and Hallam 1961) re-derived the distance to M33 by comparing a color-magnitude diagram of stars in M33 to a composite color-magnitude diagram of young galactic clusters. In 1932, Hubble reported finding 12-15 objects in M33 which he tentatively identified as globular clusters. He noted, however, that they were fainter and bluer than most globular clusters in M31 and our galaxy. Hiltner (1960) performed UBV photometry on 23 clusters, including those found by Hubble. He suggested that they might be rich galactic clusters rather than globulars, but noted that, on the other hand, they might be counterparts of the faint blue globular cluster NGC 7492 in the Milky Way. These results were corroborated by Kron and Mayall (1960), who included 4 clusters in M33 in their PV photometry. Vorontsov-Velyaminov (1955, 1956a, 1956b) found that the supergiants in M33 tended

to crowd together and form compact groups, 65 of which he catalogued. He stated that the dust in the spiral arms appeared to avoid close contact with such groups. The only trace of a Population II nucleus he could find for M33 was a feature no larger than a single globular cluster. Walker (1964, 1967) obtained an infrared plate (103a-U + RG8) of M33, with a limiting magnitude between the apparent magnitudes of Populations II and I red giants, and a blue plate (103a-O + GG13) exposed to the same density for OB stars as the infrared plate. Making a composite from the blue negative and an infrared positive, Walker brought to light the existence of a smooth, elliptical distribution of Population II red giants in M33. From this evidence he argued that M33 must be just as old as M31, and that the difference in their morphological appearance was due solely to different initial conditions.

(7) Kinematics. — Although the rotation of M33 was discovered in 1916 (Pease 1916), the first study of the rotation appeared more than two decades later (Mayall and Aller 1940, 1942). This study was based upon the radial velocities of 25 emission nebulae, determined from low-dispersion spectrograms. The rotation curve was roughly linear within 15' of the nucleus, reached a peak of $\sim$105 km/sec radial velocity ($\sim$125 km/sec circular velocity) between 15' and 20', and decreased thereafter. Models of the mass distribution responsible for the observed rotation were discussed by Wyse and Mayall (1941, 1942), Aller (1942a), Mayall (1951), Lohmann (1954), Schwarzschild (1954), Kerr and de Vaucouleurs (1956), and Takase (1957). In contrast to the situation in M31 and the Milky Way, no rapidly rotating nucleus has been seen in M33 (Walker and Fish, reported by Whitford 1962, 1963). The observations of M33 were of limited usefulness in the discussions of whether spiral arms lead or

trail in galactic rotation (Hubble 1943; Lindblad and Brahde 1946; Lindblad 1948; de Vaucouleurs 1958) because of the difficulty in determining which side of M33 is closer to the observer.

New kinematical data for M33 were added by the observations of Dieter (1962) and Volders (1959) in the 21-cm line of neutral atomic hydrogen. These observations yielded much better velocity resolution than did the optical data. However, the positional accuracy of the measurements was quite low, since the half-power beam widths of the telescopes were respectively 53' and 34'. The masses derived in the two radio studies were both significantly larger than the mass Mayall and Aller had found. Burke, Turner, and Tuve (1963) obtained 21-cm observations with angular and velocity resolution both improved over those available to Dieter and Volders, but restricted their study to the major and minor axes of M33. They found that the systemic velocities obtained from the observations along the two axes disagreed by 5 km/sec, an amount which they stated "is significant but is not understood." They did not derive a mass for M33 from their observations.

Brandt (1965) used 110 Å/mm spectrograms to determine radial velocities from the Hα emission of 24 H II regions in M33, mostly the same regions used by Mayall and Aller. Brandt's measurements indicated that the turnover point of the rotation curve lay beyond the outermost optical features within M33 (in disagreement with the earlier optical measurements). Because his measurements did not reach the turnover point of the rotation curve, he supplemented them with Dieter's and Volders' radio data, finding a total mass of $3.9 \times 10^{10}\ M_{\odot}$ for M33. He also noted that, by truncating his model at appropriate distances from the

center of the galaxy, he found "remarkably consistent" agreement between his results and all of the previous mass determinations.

The most detailed kinematical study of M33 available is by Carranza et al. (1968). Using Fabry-Perot interferograms of the Hα emission from M33, they measured 1048 points in the galaxy at dispersions of 15-30 Å/mm. They found an asymmetry between the northern and southern halves of the rotation curve; the mean of the two agreed with Brandt's measurements. Furthermore, in the southern half of the galaxy they found that the gas in the spiral arm appeared to be rotating more rapidly than the gas in the adjacent interarm region at the same distance from the nucleus.

CHAPTER II: OBSERVATIONS

Observations of M33 in the 21-cm line of neutral atomic hydrogen were made during two observing periods with the 300-foot radio telescope of the National Radio Astronomy Observatory. The first period extended over six weeks in December 1965 and January 1966; the second period over seven weeks in January, February, and March 1968. Because the 300-foot telescope is a meridian transit instrument, the observations were obtained in the form of drift curves lasting about half an hour and spaced at intervals of one sidereal day.

During the first observing period, the paraboloidal reflector was illuminated by a rectangular horn feed (E-plane NS), which produced a primary beam pattern with a width of 10' at the half-power points in both right ascension and declination. The multichannel receiver contained 21 crystal-filter channels with an average bandwidth of 95 kHz (20 km/sec) at half-power points plus two wider ($\sim$0.5 MHz) channels. The narrow channels were spaced at intervals of 100 kHz center to center. The wider channels served as monitors for signals too weak to show up in the narrow channels. The channels were frequency-switched between a 2-MHz wide signal band centered at a frequency appropriate to radiation emanating from M33 and a similar comparison band centered at 1425 MHz. The output of each channel was filtered by an RC network with a 10-second time constant, and sampled every 10 seconds by a digital voltmeter. The combination of the receiver time constant and the drift rate of the galaxy through the beam broadened the effective antenna pattern (Howard 1961) to a half-power width of 11!4 in right ascension. The readings of the voltmeter were recorded on magnetic tape. In addition, analog records

of the output of each channel were maintained in order to allow visual monitoring for interference and equipment malfunction. Before and after each observation, a neon bulb which projected slightly into the waveguide near the base of the horn was switched on to provide a calibration signal. The equivalent antenna temperature of the signal from the bulb was calibrated in the laboratory and against sources of known flux density with the total-power channel of the receiver. The system noise temperature was 200° K, and the beam efficiency of the telescope was η_B = 52%. Further details about the system have been published by Roberts (1965) and Höglund and Roberts (1965). The latter reference includes a block diagram of the receiver.

During the second observing period, a feed consisting of a pair of crossed dipoles illuminated the dish. The beam shapes and sizes were the same for both feeds, to within the errors of measurement. The half-power beam widths were 9!0 in α and 10!2 in δ. The outputs of the orthogonal polarizations were connected to separate parametric amplifiers--numbers 2 and 4 of the four-feed system (Davis and Hagstrom 1968)--each of which fed 25 channels of a 50-channel receiver (Balister 1968). This arrangement permitted the acquisition of two independent observations during each day's drift scan. The 50 filters consisted of double-tuned LC circuits yielding an average bandwidth of 97 kHz at half-power points. Each bank of 25 channels was switched between the 2.5-MHz wide signal band and a similar comparison band centered 4.0 MHz away at a lower frequency. An on-line DDP-116 computer controlled the frequency switching of the radiometer, alternating 50-msec periods at the signal and comparison frequencies. A noise tube was fired during the signal portion of every twentieth cycle. The outputs of the channels were integrated

electronically for 45-msec periods, converted to digital form, and combined numerically in the on-line computer. After 10 seconds, the results, expressed as fractions of the equivalent antenna temperature of the noise tube, were written on magnetic tape. The system noise temperatures were 150° K for both receivers. The beam efficiency of the telescope was 42%.

On 17 days of the second observing period, the 100-channel autocorrelation receiver (Weinreb 1963; Shalloway 1964) was substituted for one bank of the multichannel receiver. The physical arrangement of the receivers necessitated that the other bank of the multichannel receiver also be disconnected while observations were being obtained with the autocorrelation receiver. Two bandwidth settings, 2.5 MHz and 625 kHz, were used, yielding effective channel bandwidths of 25 kHz and 6.25 kHz, respectively.

A log of the observations is given in Table 1. For all of the observations during the first observing period, and for most during the second, the telescope was fixed in declination while the earth's rotation carried the telescope beam across the galaxy. However, on five days during the second observing period the telescope was driven southward at a constant rate while data were being obtained. The scan rate was chosen such that the telescope beam passed through the optical centers of both M31 and M33.

In the reduction of the drift curves, linear baselines were fitted to six minutes of data at each end of the scan. Baseline curvature, as evidenced by a difference between the slopes of the left and right baselines greater than an arbitrary amount, formed a criterion for rejection of individual observations. Removal of the baseline fitted to both

TABLE 1

NUMBER OF OBSERVATIONS OBTAINED AT VARIOUS DECLINATIONS

Nominal Declination Offset	Dec. 1965-Jan. 1966[a]	Jan.-Mar. 1968[b]
70' S	1	-
65' S	-	2
60' S	3	2
55' S	-	2
50' S	1	4
45' S	1	2
40' S	1	2
35' S	1	2
30' S	2	2
25' S	2	-
20' S	2	2
15' S	2	-
10' S	2	-
5' S	2	-
0'	2	2
2' N	1	-
5' N	2	-
8' N	1	5*, 2†
10' N	1	-
15' N	2	-
20' N	2	4
25' N	2	2, 5*, 2†
30' N	2	2
35' N	1	4
40' N	1	2
45' N	1	2
50' N	2	2
55' N	1	2
60' N	1	2
65' N	-	2
variable‡	-	10

a. Obtained by M.S. Roberts b. Obtained by author

* Autocorrelation receiver, 625 kHz bandwidth

† Autocorrelation receiver, 2.5 MHz bandwidth

‡ Scans along a line through the centers of M31 and M33

ends of the scan corrected for a possible linear receiver drift over the duration of the scan.

CHAPTER III: NEUTRAL HYDROGEN DISTRIBUTION

1. Mass

Figure 3 is a contour map of the integrated 21-cm line emission ($\int T_B(v_r)\, dv_r$, where T_B is brightness temperature in °K and v_r radial velocity in km/sec) from M33, and was constructed in the following manner. At each declination the channels which contained visible signals at or near the position of the galaxy were noted. The brightness temperatures in these channels, plus an additional channel at either end of the velocity range, were then summed. The signal in each channel of the sum was weighted according to the channel bandwidth. Contour levels were chosen at intervals of one-tenth of the maximum value attained in any of the resulting drift curves. The positions at which the various contour lines intersected the drift curves were determined by linear interpolation between adjacent 10-second points. Freehand contour lines were drawn connecting these positions.

Under the assumptions that (1) the galaxy is optically thin to 21-cm line radiation and (2) there is no interaction between line and continuum radiation, one may derive (e.g., Roberts 1968b) the following expression for the mass of neutral atomic hydrogen responsible for the observed 21-cm radiation:

$$M_{HI}/M_{\odot} = 1.236 \times 10^{-9}\, D^2 \iiint T_B(v_r)\, dv_r\, d\alpha\, d\delta. \qquad (3.1)$$

Here, D is the distance in parsecs and $d\alpha$ and $d\delta$ are measured in minutes of arc. Planimetry of the map in Figure 3 yields a mass of $1.4 \times 10^9\ M_{\odot}$ within the lowest contour, for an assumed distance of 720 kpc. However, there is still neutral hydrogen outside this contour. Numerical

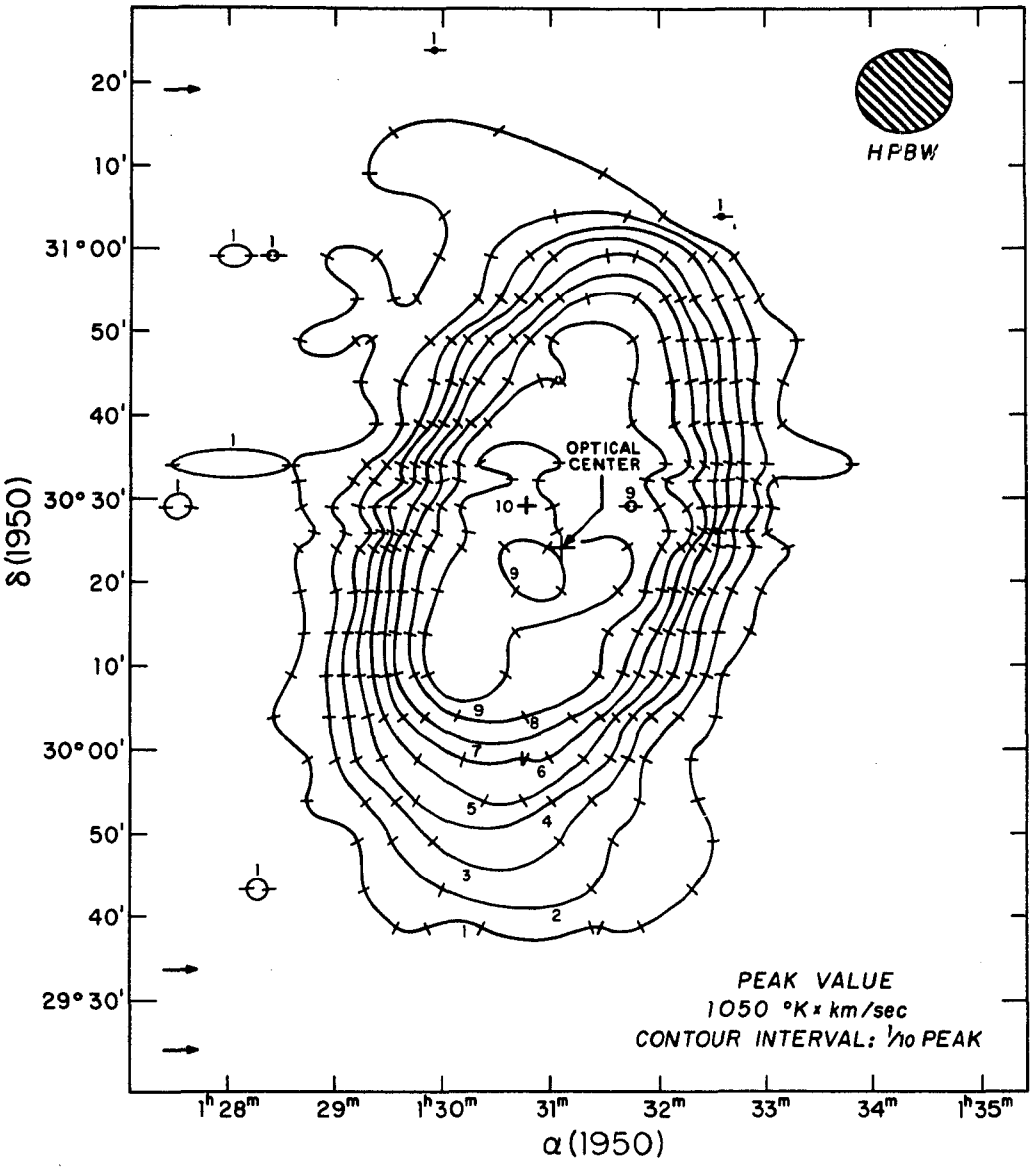


Figure 3. — Integrated 21-cm Brightness Distribution. The map contains contours of beam-averaged brightness temperature integrated over all velocities appropriate to line emission from M33. The three arrows at the left of the map indicate declinations at which scans were obtained which remained below the level of the lowest contour.

integration over a region 2° in diameter in declination by 8^m in right ascension (about three times the area of the lowest contour in Fig. 3) yields $1.6 \times 10^9 M_\odot$. Increasing the EW diameter of the region by 25% changes the value of the integral by less than 1%. The mass of neutral atomic hydrogen may thus be considered known to within an estimated mean error of $\pm$ 10%, the uncertainty arising primarily from the calibration of the brightness temperature scale. The present value may be compared with values of $M_{HI}/M_\odot = 1.3 \times 10^9$ (Volders 1959), 1.3×10^9 (Dieter 1962), and 2.4×10^9 (Meng 1968) obtained in previous studies. These values have been corrected for differences in the assumed distance to M33.

2. Form of the Distribution

From the contours of Figure 3 it can be seen that the distribution of beam-averaged 21-cm brightness temperature is flat-topped with a central depression. Although the depth of this central depression is only about 10% of the maximum brightness in Figure 3, its reality is not in doubt. Every one of the drift curves between declinations 5' N and 10' S of the optical center used in the construction of the contour map is double peaked, while the drift curves outside this declination range are all single peaked.

If one takes advantage of the ordered motions existing within galaxies, one can restrict the region of the galaxy from which signals are received to a source which is narrower in one dimension than the beam. This technique will be discussed in more detail in Chapter IV. Figure 4 shows cross sections parallel to the minor axis of M33 of contour maps constructed from the responses of the individual 20 km/sec wide channels. The major-axis positions were chosen such that the cross sections go

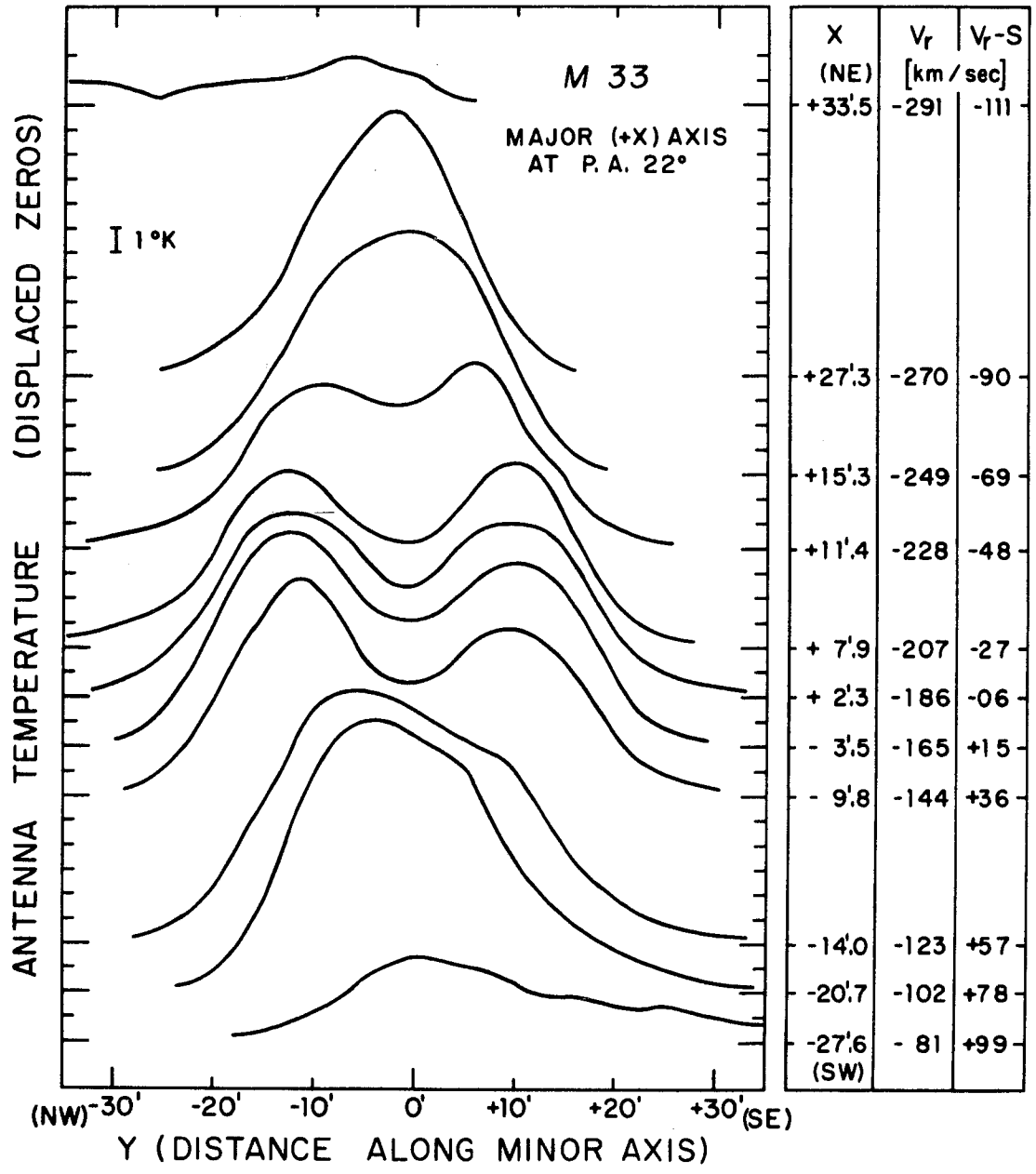


Figure 4. — Cross Sections of Individual-Channel Brightness Distributions parallel to the minor axis of M33 reveal both the sense of rotation of the galaxy and the ring-shaped character of the neutral-hydrogen distribution. The sections are labeled with the channel velocity (both with respect to the sun and to the systemic velocity of M33) and the position (X) at which they intersect the major axis.

through the peaks of the individual contour maps. The depth of the central depression is somewhat emphasized in this technique, by an amount which depends upon the kinematics of the galaxy. However, it will be shown that the central depression cannot be attributed to effects of the kinematics alone, and that the shape of the neutral hydrogen distribution can best be described as a broad ring.

Two more features of the hydrogen distribution are worthy of note. Its center is displaced from the optical center of the galaxy by several minutes of arc. Since the pointing accuracy of the 300-foot telescope is better than $\pm$ 1', this effect is real. Also, there are departures from axial symmetry. In particular, the NE and SW quadrants of the ring contain more hydrogen than do the SE and NW quadrants. This can be seen from the difference in height of the two peaks in Figure 4 for a given channel. A second type of departure from axial symmetry can be seen in the wings extending from the NW and SE ends of the galaxy in Figure 3.

3. Comparison with the Distributions of Other Galactic Constituents

a) Star Counts

The star counts upon which Figure 5 is based were made by de Vaucouleurs on unfiltered 103a-O plates taken with the 20-inch Carnegie astrograph, and were very kindly made available to me (de Vaucouleurs 1968) in advance of publication. The limiting magnitude of the counts is $m_{pg} = 20.2$ over most of the galaxy, but in the central region crowding of images and the strong background of unresolved fainter stars may make the effective limiting magnitude as much as a magnitude brighter. The star counts cover the region $-30' \leq \Delta\alpha \leq 30'$, $-36 \leq \Delta\delta \leq 40'$ with respect to the

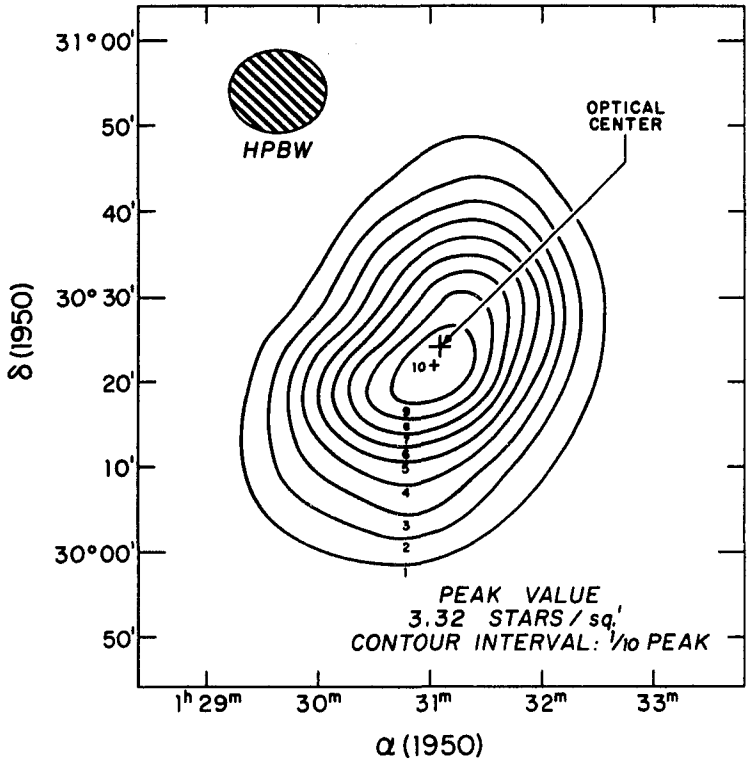


Figure 5. — Distribution of Stars Brighter than $m_{pg} = 20.2$. The contours show the distribution of luminous stars in M33 (de Vaucouleurs 1968), smoothed to the resolution of the 21-cm data.

center of M33. They were corrected for a mean foreground level, obtained by averaging the counts from the portion of the region outside the faintest contour of the photoelectric photometry (de Vaucouleurs 1959, see below), and were presented as the number of stars within squares 2' on a side. This finite resolution was taken into account when numerically convolving the data with a Gaussian beam to achieve the same resolution as the 21-cm data in Figure 3. The star counts place 2136 stars in M33. Planimetry of Figure 5 accounts for 2004 of these within the lowest contour.

The apparent blue distance modulus for M33 is $m_B - M_B = 24.6$ (de Vaucouleurs 1966). Since $m_B = m_{pg} + 0.11$ (Johnson and Morgan 1953), the counts down to $m_{pg} = 20.2$ include stars intrinsically brighter than $M_B = -4.3$. Thus the contribution from the main sequence is restricted to stars of spectral type B0 and earlier (Blaauw 1963). Stars of later spectral types must be supergiants.

b) B Photometry

The contour map of surface brightness in the B filter of the UBV system (Fig. 6) is based upon the contour diagram in de Vaucouleurs' (1959) photoelectric study of M33. Points were read from the published map at intervals of 2!5 in both right ascension and declination; these points were then numerically convolved to yield the same resolution as is shown in the 21-cm contour map (Fig. 3). The diameter of the diaphragm used in the original photoelectric observations, 2!3, was taken into account in the convolution. Planimetry of Figure 6 yields $m_B = 6.44$ within the outermost contour. The extrapolated total magnitude is $m_B = 6.27$.

An effort was made to see what types of stars contribute to the observed B light distribution and, in particular, how much this light distribution was influenced by the stars included in the star counts

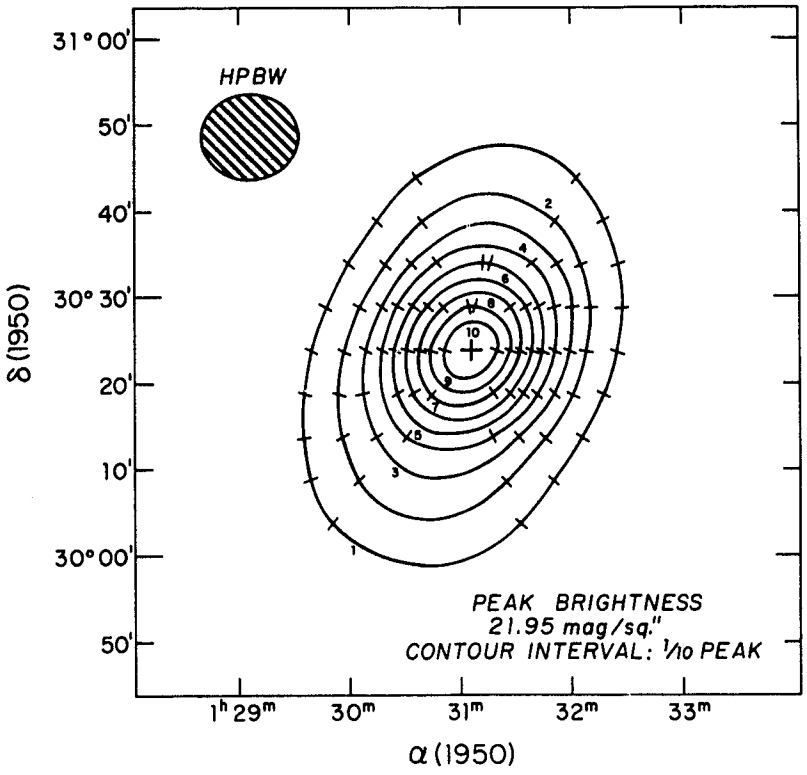


Figure 6. — B Photometry. The contours were constructed from the data of de Vaucouleurs (1959), and smoothed to the resolution of the 21-cm data.

described above. Luminosity functions were taken from van Rhijn's (1936) description of the solar neighborhood, from Sandage's (1958) discussion of the initial luminosity function Ψ ("Salpeter function"), and from Wood's (1966) multicolor photometry of galaxies. Although papers by Luyten and by McCuskey have made minor revisions to van Rhijn's values for $M_{pg} \gtrsim -2.5$, these more recent works did not consider the bright end of the luminosity function and are therefore of limited use in the present connection. Four of Wood's models were investigated: the solar neighborhood, an Sb spiral arm (from observations of M31 and M81), the central region of M51, and a spiral arm in M51. (M51 is the only Sc galaxy for which Wood presented a luminosity function.) The van Rhijn luminosity function and the first three Wood models agree in assigning less than 10% of the light in the B filter to stars luminous enough to have been included in the star counts in M33. In contrast, the intial luminosity function assigns about 40% of the light to such stars; and the luminosity function for the M51 spiral arm, which includes a comparatively large proportion of OB stars and significant numbers of blue supergiants, assigns nearly 50% of the light to such stars. In contrast to M51, M33 is a low-surface-brightness object. It is likely, therefore, that the luminosity function of M33 is intermediate between the two extremes described above. Thus most of the light mapped in Figure 6 originated from stars too faint to be counted.

c) Ionized Hydrogen

The H II regions catalogued by Aller (1954, 1956), Sĕrsic (1959a), and Courtès and Cruvellier (1965) form the basis of the contours in Figure 7. In an attempt to make the contours reflect the distribution of ionized hydrogen, each catalogued region was weighted by $[d_1 \times d_2]^{1.5}$,

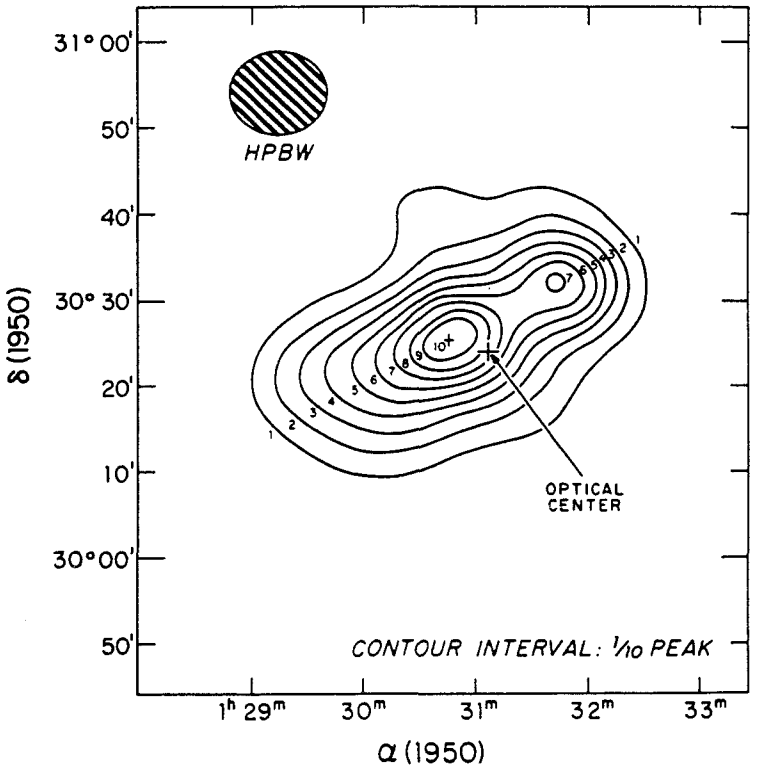


Figure 7. — Distribution of Hα Emission Regions. The contours represent the distribution of catalogued emission regions in M33 weighted by size in order to reflect as accurately as possible the distribution of ionized hydrogen as seen with the same resolution as the 21-cm data.

where d_1 and d_2 are the major and minor diameters of the H II region. These weights should be proportional to their volumes and thus to their H II content, if one neglects statistical fluctuations caused by the irregular shapes of the regions, and those caused by variations in the mean density of ionized hydrogen within the H II regions. Although this procedure is the best estimate of the distribution presently available, it suffers from several shortcomings. First are the uncertainties outlined above. Second is the incompleteness of the catalogs. Finally, even if the catalogs were complete, they would still overlook the diffuse background of ionized hydrogen outside the H II regions of classical appearance (Carranza et al. 1968). In order to overcome these deficiencies, future studies of the H II distribution should be based upon surface photometry with an Hα interference filter.

d) Discussion

The most striking difference between the H I distribution and the distributions of the other constituents of the galaxy is the much greater extent of the neutral hydrogen. The diameter of the outermost contour (at a level 0.1 of the observed peak of the distribution) of the 21-cm brightness distribution is 93', while the corresponding figures for Figures 5-7 are approximately 50'. Table 2 displays these comparisons in greater detail and contains, in addition, the diameters of continuum radio-frequency contours from the two studies made with 10' beams (Venugopal 1963; DeJong 1967).

The second difference is in the forms of the various distributions. While three of the distributions are centrally condensed, the neutral-hydrogen contours reflect a flat-topped distribution with a central

TABLE 2

OBSERVED DIAMETERS AND OFFSETS OF M33 CONSTITUENT DISTRIBUTIONS

Constituent	Diameter at 0.5 x peak		Diameter at 0.1 x peak		Offset	
	Major	Minor	Major	Minor	$\Delta\alpha$	$\Delta\delta$
Integrated neutral hydrogen	67'	36'	93'	56'	-3'	-2'
Optical continuum (B filter):						
observed (de Vaucouleurs 1959)	7	5	33	19	0	0
smeared	21	16	50	34	0	0
Star counts, smeared (de Vaucouleurs 1968)	29	19	52	35	-1	-2
H II regions, smeared:						
weighted	29	12	47	26	-5	+1
counts	26	17	42	32	-1	-2
Radio continuum:						
1410 MHz (Venugopal 1963)	34	26	-	-	-	-
2695 MHz (DeJong 1967)	28	20	-	-	0	0

depression. This is illustrated in Figure 8, which is a graph of the fraction of a particular distribution contained within a given contour. This graph is essentially independent of the sizes of the distributions and reflects only their shapes. A two-dimensional Gaussian distribution would produce a straight line on the graph. For this reason, the Gaussian distribution forms a convenient standard for comparison with the observed distributions. Also, many distributions in nature can be quite well approximated by a Gaussian function. The flat-topped character of the H I distribution is shown by the deviation above the diagonal of the points referring to the inner H I contours. The deviation below the diagonal of the points referring to the inner B-photometry and H II-region contours indicate that these distributions are more centrally condensed than a Gaussian.

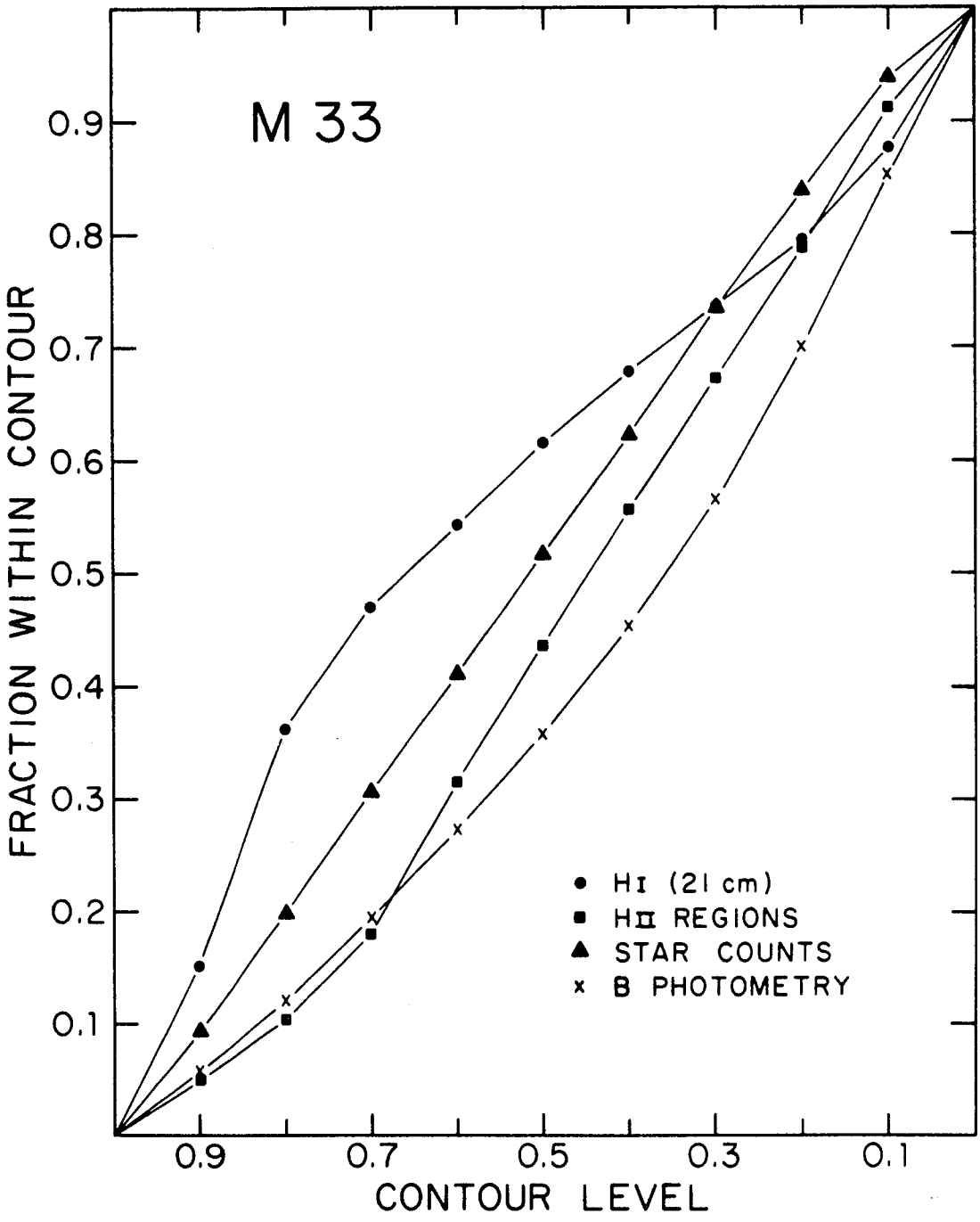


Figure 8. — Comparison of the Constituent Distributions. The fraction of a constituent distribution contained within a given contour level is an index of the shape of the distribution, but is independent of its angular size.

The fact that the points referring to the outer contours of the H I and B-photometry distributions fall below the diagonal indicates that these distributions have tails which are stronger than would conform to a Gaussian distribution. In the case of the photometry, this is to be expected, since both Patterson (1940) and de Vaucouleurs (1959) found that the outer parts of the light distribution decayed exponentially with distance from the galactic center. In the case of the 21-cm data, the result may be ascribed to the effects of the wings visible on the north-preceding (np) and south-following (sf) ends of M33. The star counts, on the other hand, cut off more sharply than would be predicted by a Gaussian distribution.

A third noteworthy feature of the distributions is the fact that only the B photometry is centered at what is commonly considered to be the optical center of the galaxy. The centers of both the 21-cm and star-count distributions are displaced to the south and west of this center. The peaks of the distribution of the Hα emission are determined primarily by the heavily weighted H II regions with NGC numbers. However, if the H II regions are weighted equally rather than by size, the peak of their distribution also lies south and west of the optical center of M33. The displacements of the centers of the various distributions are listed in Table 2.

In our own galaxy, O stars, H II regions, and interstellar neutral hydrogen are considered to belong to the extreme Population I, while the fainter stars that contribute most to the light to the B photometry are assigned to older population groups. The displacement of the centers of the different distributions raises several questions. Is this unique to M33 or a common phenomenon? Is the displacement of several

hundred parsecs the result of a fairly quiet perturbation, and cyclical in nature? Or is it the aftermath of a single cataclysmic event in the evolution of the galaxy? These questions cannot be answered by looking only at the forms of the various distributions. However, the frequency resolution of spectral-line observations provides information about the kinematics of the galaxy, yielding additional clues to these problems.

4. Search for a Neutral-Atomic-Hydrogen Link Between M31 and M33

Observations in the 21-cm spectral line have shown that, as a general rule, the neutral atomic hydrogen associated with spiral and irregular galaxies extends throughout a much larger region of space than do any of the optically detectable components of the galaxy. As a result, there have already been cases where an H I bridge has been found linking galaxies which appear close together but separate optically. The first of these cases to be reported was the common envelope of the Magellanic Clouds (Hindman, Kerr, and McGee 1963). More recently, Roberts (1968a) found a bridge between the galaxies NGC 4631 and NGC 4656. Also, Strauss (1968) reported tracing an extension of an outer spiral arm of our galaxy more than half way from the Milky Way to the Small Magellanic Cloud. However, reobservation with improved equipment failed to confirm the original detection of this feature (Turner 1968).

Within the Local Group (see Fig. 9) one can recognize two major subgroups: one dominated by the Milky Way, and the other by Messier 31. Messier 33 lies quite close to M31; the distance between them is 15°.3 as seen on the plane of the sky. This translates into a linear separation of 190 kpc if one accepts distances of 690 kpc for M31 and 720 kpc for M33 (de Vaucouleurs 1966). This separation is 5 times the minimum separation between NGC 4631 and 4656, and about 4 times the distance

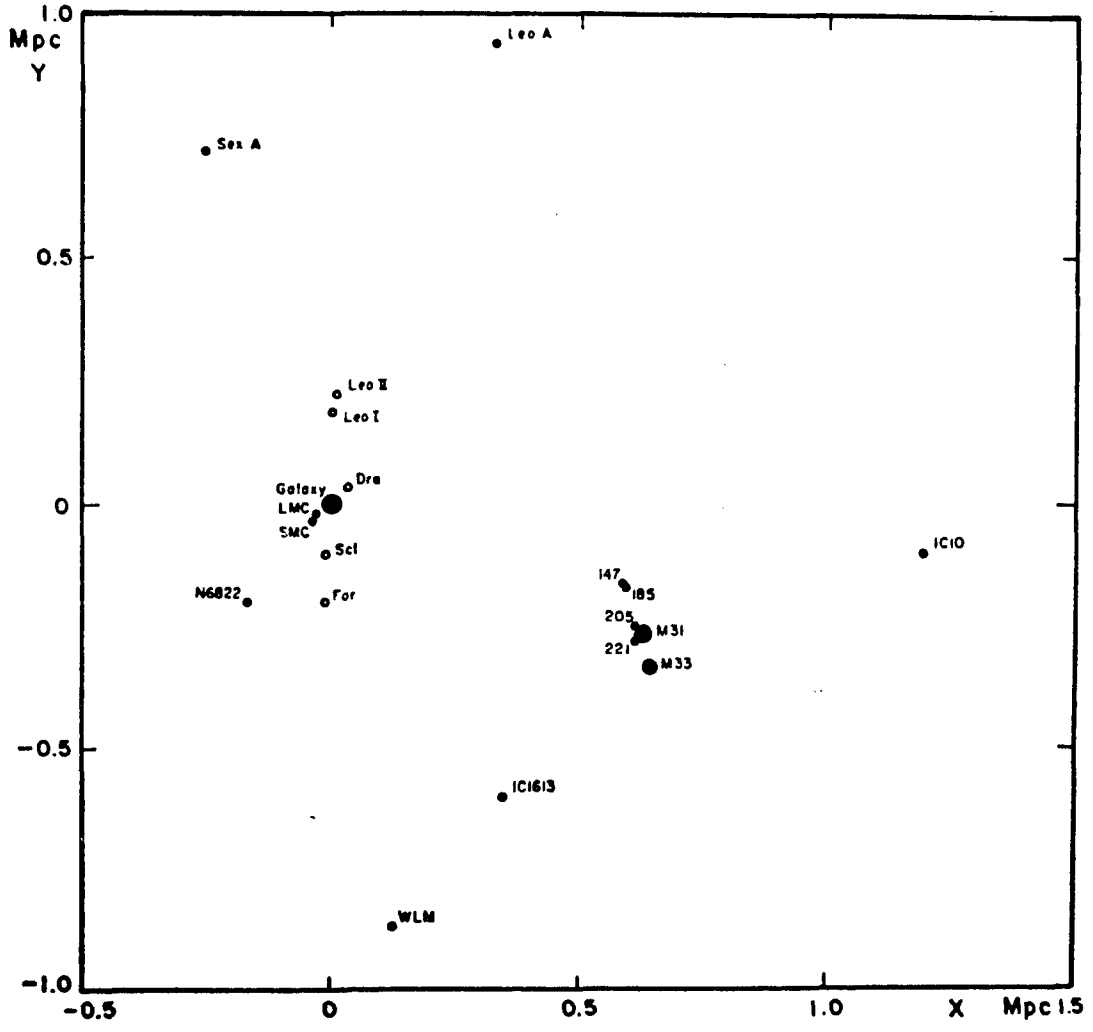


Figure 9. — Local Group Projected into the Supergalactic Plane. The positions of galaxies in the Local Group projected into the plane defined by the great circle toward which the brighter galaxies are concentrated. The supergalactic plane has its north pole at $\ell^I = 15°$, $b^I = +5°$, and longitudes are reckoned from the line of nodes, OX, with the galactic plane at $\ell^I = 105°$, $b^I = 0°$ (from de Vaucouleurs and Ables 1965).

from us to the Magellanic Clouds. In terms of the galaxies themselves, the separation is roughly 4 times the diameter of M31 and 10 times the diameter of M33.

Observations were obtained on 5 days in February 1968 (see Table 1). The drift scans lasted for an hour and a quarter; and during this time the telescope was driven southward at a constant rate such that the beam passed through the centers of M31 and M33 as they transited. The signals were integrated for 10 seconds at a time, yielding 450 readings per channel per scan. Because of the large number of data points and limited space in the computer, the scans had to be reduced either in two sections or with pairs of adjacent points averaged together. In practice, both methods were carried out, and their results compared.

Since no signals could be recognized in the drift curves of the individual 20 km/sec-wide channels, adjacent channels were averaged together. This procedure will be effective if signals are being emitted from regions in which the velocity dispersion is larger than the channel bandwidth. Figure 10 shows the results of averaging channels in groups of five, for an effective bandwidth of 0.5 MHz or 105 km/sec. In addition to the centers of M31 and M33, the position of the lenticular galaxy NGC 404, which happens to lie within 2' of the scan line, is indicated. The vertical scale is labelled in units of the product of brightness temperature and bandwidth. Since the bandwidth is about 100 km/sec, the height of one box is roughly equivalent to 1° K. There are no convincing signals in these drift curves, except for those seen in the directions of the 3 galaxies. The noisy nature of the lowest scan is caused by irregularities in local foreground hydrogen.

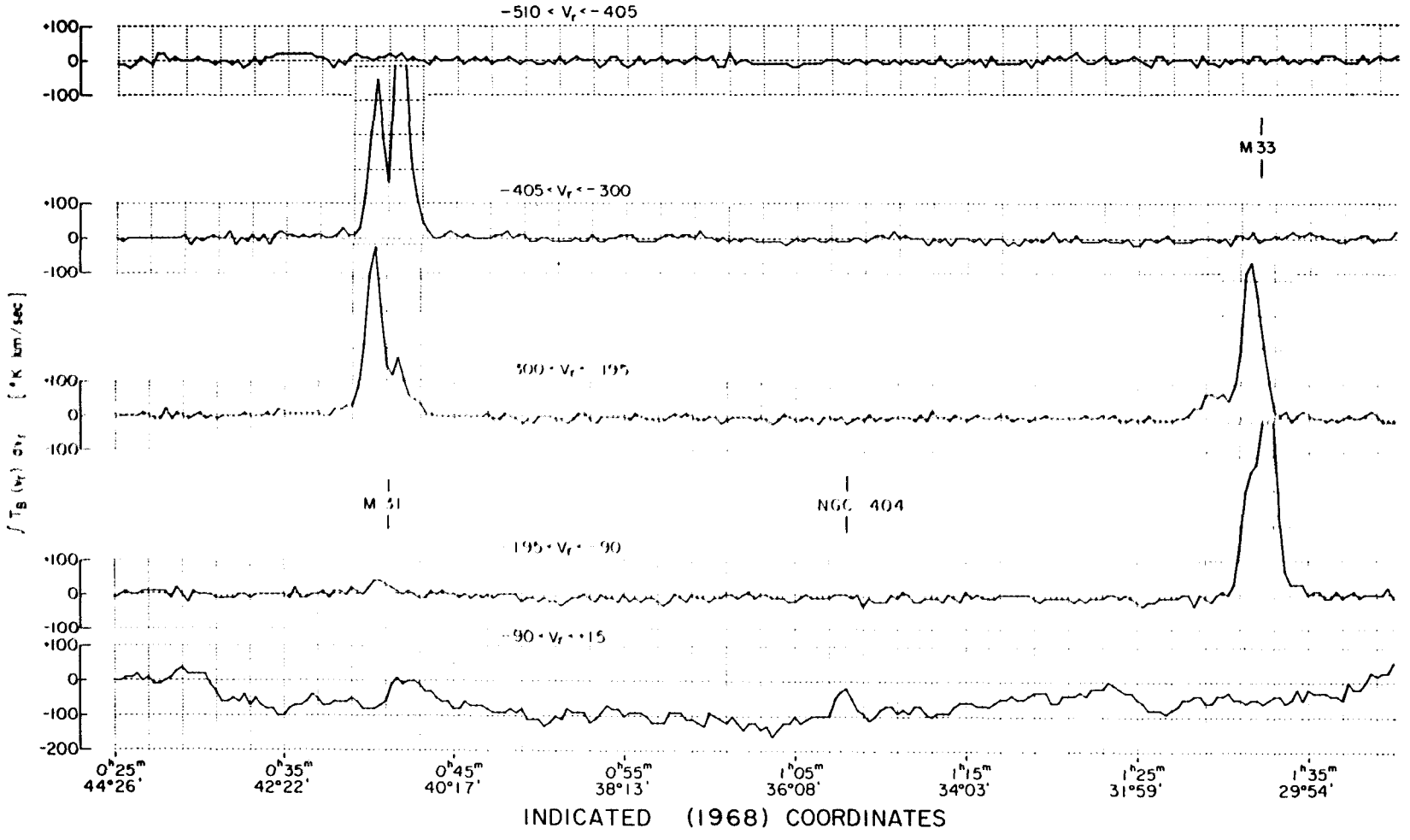


Figure 10. — Drift Scans through M31 and M33. Each scan represents the sum of five adjacent channels. The centers of M31 ($\alpha_i = 0^h\ 41^m\ 05^s$, $\delta_i = +41°\ 05'.8$) and M33 ($\alpha_i = 1^h\ 32^m\ 15^s$, $\delta_i = +30°\ 28'.2$) are indicated, as well as the closest approach of the scan to the lenticular galaxy NGC 404.

Summation of points along the scan channel by channel yields a velocity profile. The points in the intergalactic region, from $0^h\ 45^m$ to $1^h\ 27^m$, were used to create the profiles in Figure 11. The dashed curve is for data from the scans reduced in two sections, the solid curve from the reduction by means of averaging adjacent points. The last few channels suffer from confusion with foreground hydrogen. The negative bias of the latter profile probably results from a slight curvature of the baseline. The scatter of the points is only slightly larger than would be expected from the noise in the system, and there is only one point among the first 20 channels which falls more than 2σ away from the mean for those channels. Hydrogen in the region between the galaxies might have been expected to show up particularly in channels 10 to 16, which cover the range of radial velocities between the systemic velocities of M31 and M33.

The number of neutral hydrogen atoms in a square-centimeter column is proportional to the integrated 21-cm brightness temperature. Adopting 30° K km/sec (which is four times the r.m.s. scatter in the top four drift curves of Fig. 10) as an upper limit for the integrated brightness temperature in the bridge leads to an upper limit of 5×10^{14} atoms/cm^2 on the surface number density of H I. This upper limit is roughly four times lower than the observed brightness temperature of the bridge between NGC 4631 and 4656. It corresponds to an upper limit of $1.6 \times 10^8\ M_\odot$ of neutral hydrogen in the surveyed area, a strip 10' wide and 15° long between M31 and M33.

If a bridge does exist between M31 and M33, and if it is a cylinder with the same linear cross section as Roberts found for the bridge between NGC 4631 and NGC 4656, then the bridge should appear 6 times as

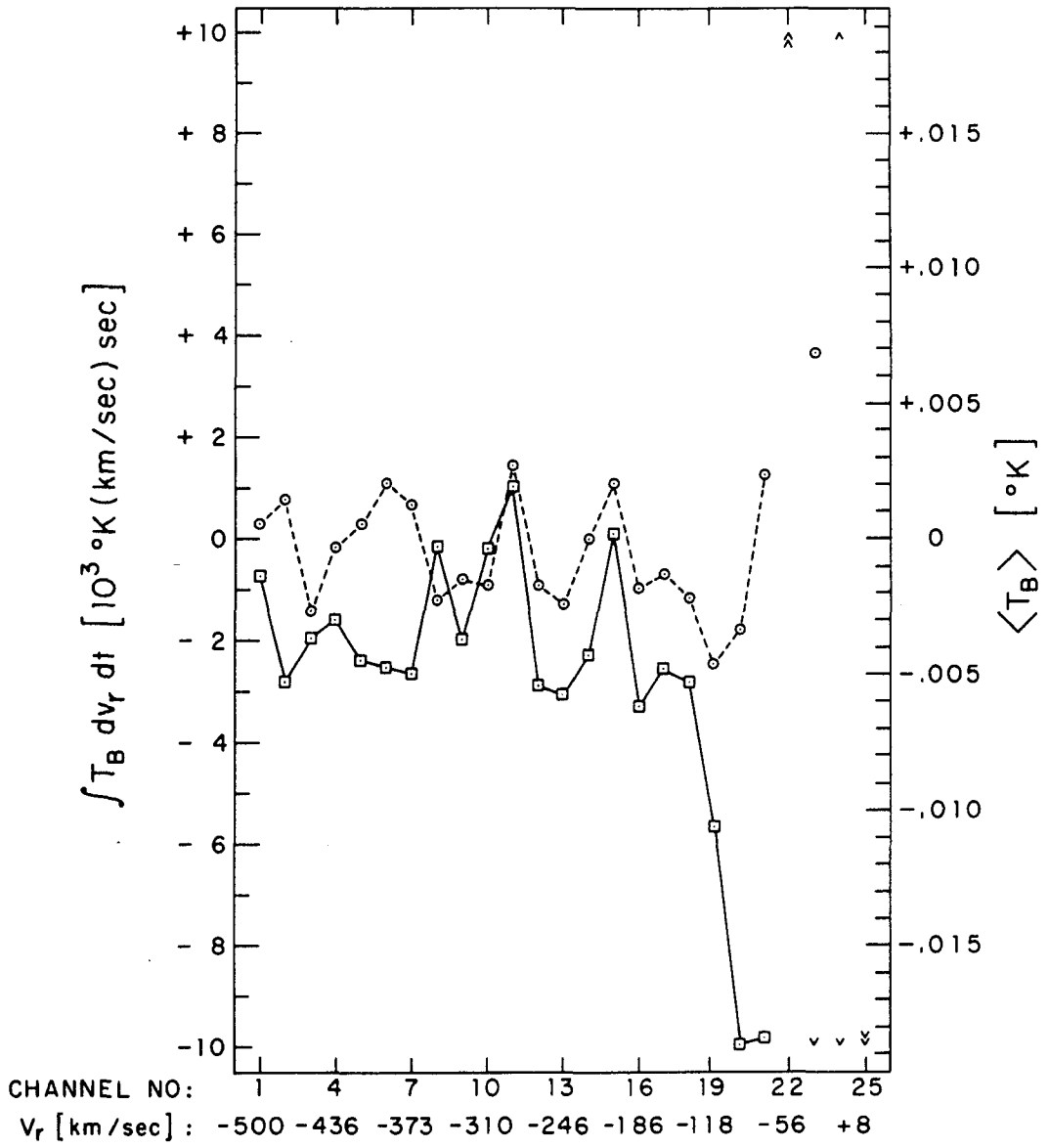


Figure 11. — Velocity Profile of the Intergalactic Region. The profiles were created by summing each channel from $\alpha_i = 0^h\ 45^m$ to $\alpha_i = 1^h\ 27^m$. The solid curve is from the data reduced by means of averaging adjacent points, the dashed curve from the data reduced in two sections. The discrepancy between the two profiles is caused by the different methods of removing the baseline. This figure confirms the lack of appreciable signals apparent from Fig. 10.

broad as the surveyed area. Hence, the upper limit for its H I mass is 10^9 $M_\odot$ or less than 19% of the mass of neutral atomic hydrogen in M31 and M33 proper. The mean excess density of neutral hydrogen in the bridge, above the density of the general extragalactic medium, would be less than 1.2×10^{-8} atoms/cm^3, or 2×10^{-32} grams/cm^3 (an order of magnitude lower than the mean density of the intergalactic medium; McVittie 1965).

A comparative listing of the parameters of the three pairs of galaxies (the Magellanic Clouds, NGC 4631/4656, and M31/M33) is given in Table 3. The values for the masses of the Magellanic Clouds refer only to the "main bodies" of the galaxies, and the value for the bridge refers to the "envelope" of the galaxies--of which perhaps half should be considered as forming the bridge and the rest as belonging to the individual Clouds.

TABLE 3

COMPARISON OF INTERGALACTIC H I BRIDGES

Parameter		LMC/SMC	NGC 4631/4656	M31/M33
Distance (assumed)		46 kpc	4 Mpc	700 kpc
$M_{HI}/M_\odot$	galaxy a	3.2×10^8	4.0×10^9	3.7×10^9
	galaxy b	2.8×10^8	1.4×10^9	1.6×10^9
	bridge	4.0×10^8	0.7×10^9	$<1.0 \times 10^9$
	complete system	1.0×10^9	6.4×10^9	$<6.3 \times 10^9$
% H I mass in bridge		40(20)	11	<16
$\int T_B dV$ in bridge [°K km/sec]		170	120	<30

CHAPTER IV: KINEMATICS

1. General Considerations and Assumptions

In order to describe completely the kinematics of a galaxy, one would have to set up a mass or density function of six independent phase-space coordinates--three positions and three velocities. However, all observational quantities are functions of only three coordinates--positions projected against the celestial sphere, and radial velocity. In order to make any headway in the description of galaxy kinematics, one must invoke symmetry arguments to reduce the number of independent variables. The particular symmetries used are derived from observational experience and from the assumption that galaxies form a class of objects with many properties in common.

The two primary assumptions generally made are that spiral galaxies are highly flattened objects, describable in the limit as planes of infinitesimal thickness, and that they are axially symmetrical about axes perpendicular to their primary planes. While the stellar content of Sb and Sc galaxies seen edge-on displays a distribution with an axial ratio typically in the range of $0.2 \gtrsim c/a \gtrsim 0.1$, the gas and dust have an even flatter distribution. In our own galaxy, for example, the neutral hydrogen within $R_o = 10$ kpc forms a layer with a full width at half density of 160-220 pc (corresponding to $c/a \sim 0.02$) and a deviation from the central plane of $\lesssim 25$ pc (Kerr and Westerhout 1965). It is only outside the circle corresponding to the solar distance from the galactic center that the hydrogen layer begins to thicken and to become subject to the "hatbrim effect". The thinness and flatness assumption should therefore be quite a reasonable approximation to the true state

of affairs; and minor corrections to values obtained on the basis of this assumption can be applied to account for the effects of finite thickness.

The assumption of circular symmetry appears to be at least roughly satisfied in all normal spiral galaxies. For this reason, and because of the simplicity of circular as opposed to noncircular models, circularly symmetric models are used as a starting point in the fitting of models to the data. The departures of the data from circular symmetry can then be described by differences in parameters obtained for various subsets of the data.

The derivation of the kinematics of galaxies from observations at 21-cm wavelength is hampered by the limited angular resolution of radio telescopes. Rotation curves obtained from observed position-velocity loci are distorted by the effects of beam smearing. Roberts (1968a) has shown how severe the distortion is in the case of a galaxy with a diameter approximately twice the half-power beamwidth of the telescope. In the case of M33, where the radio diameter is at least six times the half-power beamwidth, the effects of beam smearing are not nearly as serious. However, it is still true that, because of the interplay of a large number of parameters in the creation of a position-velocity locus or rotation curve, the corrections for beam smearing must be made on the original observed data. One such approach would involve a two-dimensional deconvolution of antenna-temperature contours for each of the observed velocity intervals. The danger of this approach is that the process of deconvolution forces a deterioration of the signal-to-noise ratio of the data. As a result, some of the features in the deconvolved picture of the data may in fact be spurious, even though

resmearing of the deconvolved picture produces very small departures from the observed data. An example of such a spurious feature is the strong central peak originally found (van de Hulst, Raimond, and van Woerden 1957) in the density distribution of neutral hydrogen in M31, which is not present in observations obtained with higher resolution (Roberts 1966). An alternative method, adopted here, is to construct simplified but reasonable models of a galaxy, smear them numerically, and choose from these models the one which best fits the data.

2. The Model-Fitting Program

The purpose of the computer program is to take a circularly symmetrical thin-disk model of the galaxy with known hydrogen distribution, rotation curve, and orientation; to convolve this model with a circular Gaussian beam and a number of narrow filters, thereby simulating the smearing action of the telescope and receiver; and to determine the r.m.s. deviation of the resulting model drift curves from the observed drift curves.

a) Coordinate Systems

Consider the following four coordinate systems, illustrated in Figure 12:

(1) ξ, η: rectangular, in plane of the sky, origin at center of galaxy

(2) ρ, ϕ: polar, in plane of the sky, origin at center of antenna beam

(3) x, y: rectangular, in principal plane of galaxy, origin at center of galaxy

(4) r, θ: polar, in principal plane of galaxy, origin at center of galaxy

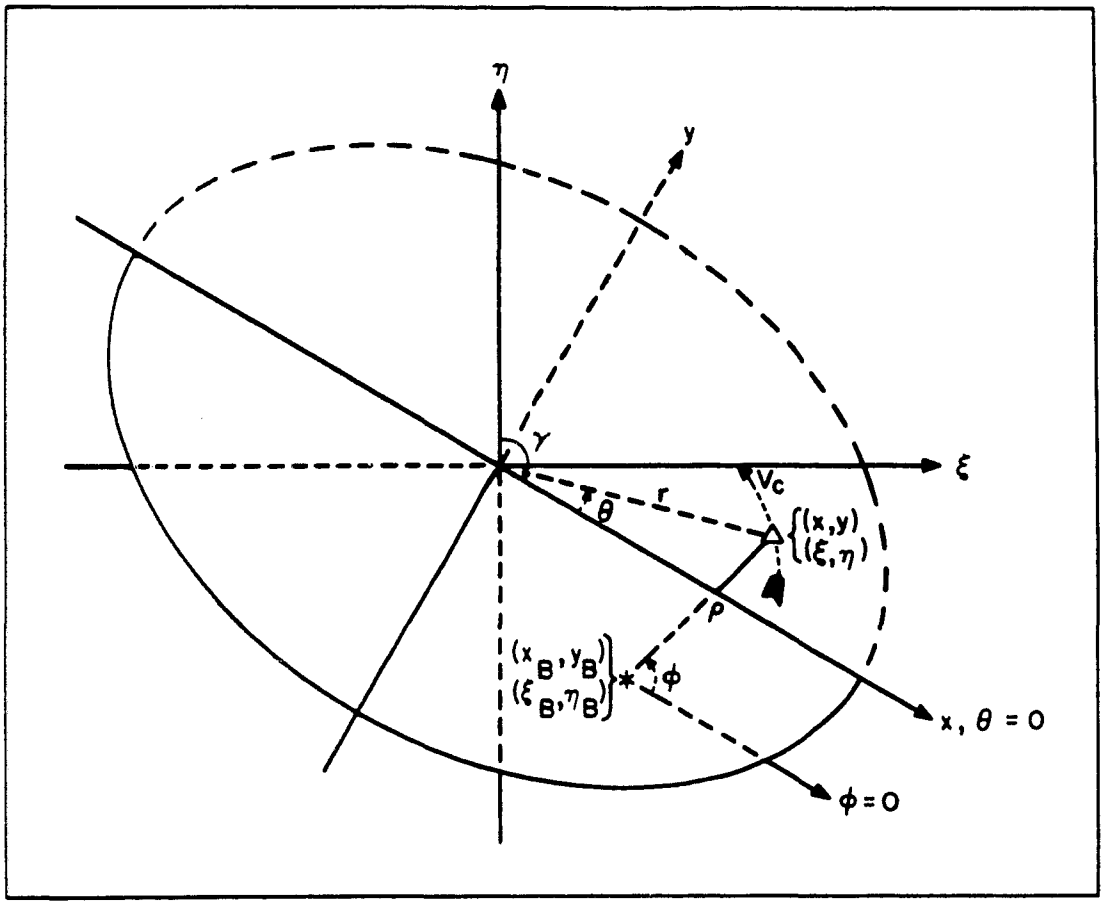


Figure 12. — Coordinate Systems Used in the Model-Fitting Program. The coordinates and the conversions between coordinates are described in the text. The ellipse represents the projected outline of a circular galaxy, Δ represents an arbitrary point in the galaxy, and * represents the center of the antenna beam.

The plane of the galaxy intersects the plane of the sky along the x-axis ($\theta = 0$ axis), which is the major axis of the galaxy or, more precisely, of its image projected on the plane of the sky. The +x axis makes an angle γ as measured from the $+\eta$ axis around through the $+\xi$ axis (i.e., clockwise, if ξ and η are plotted as a right-hand coordinate system). Thus the +x axis is the eastern half of the major axis of the galaxy. The +y axis is the northern half of the minor axis. The $\phi = 0$ axis is parallel to the +x axis; ϕ and θ are both measured counter-clockwise. The inclination angle (i) between the two principal planes is measured from the sky to the +y axis, positive away from the observer. Rotational motions (V_c) are considered positive if they occur in the sense of increasing θ, i.e., from the +x axis through the +y axis.

The following relationships represent the conversions between the coordinate systems:

$(\xi,\eta) \rightarrow (x,y)$:

$$\begin{aligned} x &= \eta \cos\gamma + \xi \sin\gamma \\ y &= (\eta \sin\gamma - \xi \cos\gamma)/\cos i \end{aligned} \tag{4.1}$$

$(r,\theta) \rightarrow (x,y)$:

$$\begin{aligned} x &= r \cos\theta \\ y &= r \sin\theta \end{aligned} \tag{4.2}$$

$(\rho,\phi) \rightarrow (x,y)$:

$$\begin{aligned} x &= x_B + \rho \cos\phi \\ y &= y_B + \rho \sin\phi/\cos i \end{aligned} \tag{4.3}$$

b) Parameters of the Model Galaxy

(1) Kinematics. — Assume a rotation curve, which gives circular velocity in the plane of the galaxy as a function of galactocentric

distance, having a form first suggested by Brandt (1960):

$$V_c(r) = \frac{A\, r}{[1 + (Br)^n]^{3/2n}} \quad , \tag{4.4}$$

where A, B, and n are arbitrary constants. This equation can be re-written in a form which makes the rotation curve somewhat easier to visualize:

$$V_c(r) = \frac{(r/R_m)\ V_m \text{ cosec } i}{\left[\frac{1}{3} + \frac{2}{3}(r/R_m)^n\right]^{3/2n}} \quad . \tag{4.5}$$

The three parameters V_m cosec i (the maximum circular velocity), R_m (the distance from the center of the galaxy to the radius at which V_m occurs), and n (an index of the breadth of the plateau region of the rotation curve) determine the rotational velocity for all values of r. Also allow expansion velocities in the plane of the galaxy of the form

$$E(r) = E_o\, r^K \quad . \tag{4.6}$$

These yield a radial-velocity field, for a galaxy with systemic radial velocity S, of

$$\begin{aligned} V_r(r,\theta) &= V_c(r) \sin i \cos\theta + E(r) \sin i \sin\theta + S \\ &= \frac{(V_m/R_m)\ r \cos\theta}{\left[\frac{1}{3} + \frac{2}{3}(r/R_m)^n\right]^{3/2n}} + E_o\, r^K \sin i \sin\theta + S. \end{aligned} \tag{4.7}$$

Finally, assume a Gaussian velocity dispersion with a constant standard deviation σ_v in radial velocity at all points.

(2) Hydrogen Distribution. — Assume a Gaussian ring of radius r_o and width σ_H, sitting on a uniform disk of radius $r_D > 0$. The surface density of neutral atomic hydrogen is then

$$H(r) = \begin{cases} H_o \exp\left[-(r-r_o)^2/2\sigma_H^2\right] + H_D & \text{for } r < r_D \\ H_o \exp\left[-(r-r_o)^2/2\sigma_H^2\right] & r \geq r_D \end{cases} \tag{4.8}$$

The parameters H_o and H_D determine the relative surface densities of hydrogen associated with the ring and disk distributions, respectively. By the choice of $r_o = 0$, the Gaussian ring becomes a central Gaussian distribution. If the hydrogen is everywhere optically thin to 21-cm line radiation and there is no interaction between line and continuum radiation, then the amount of line radiation emitted will be proportional to the surface density of neutral hydrogen atoms.

c) Parameters of the Receiving System

(1) Antenna beam. — Assume a circular Gaussian antenna pattern: $A(\rho) = \exp\left[-\rho^2/2\sigma_B^2\right]$, where $\sigma_B = \text{HPBW}/\ 2\sqrt{2 \cdot \ln 2}$.

(2) Filter bandpass. — Assume for each filter a rectangular frequency response with high- and low-frequency cutoffs v_H and v_L in terms of radial velocity, and that v_H for one channel is equal to v_L for the adjacent channel.

d) The Channel Receptivity Field

If the hydrogen in the galaxy were subject only to large-scale ordered motions with no velocity dispersion, the radial-velocity loci corresponding to v_H and v_L would define a strip in the galaxy inside of which all hydrogen atoms would emit 21-cm radiation of frequencies

accepted by the filter and outside of which no hydrogen atoms would emit acceptable 21-cm line radiation. The channel receptivity field, $F(r,\theta)$, would then resemble one of the shaded strips in Figure 13, having a value of unity inside the shaded strip and a value of zero outside.

Since, however, the hydrogen in the galaxy has a non-zero velocity dispersion, the channel receptivity $F(r,\theta)$ will not be a discontinuous function. It will instead be a function whose value is the area between v_L and v_H under a normal error curve with parameter σ_v centered at $V_r(r,\theta)$, this area being the fraction (percentage) of hydrogen atoms at a given (r,θ) which have radial velocities such that their 21-cm radiation can be accepted by the filter. Thus

$$F(r,\theta) = \frac{1}{\sigma_v \sqrt{2\pi}} \int_{v_L}^{v_H} \exp\left[-(v-V_r)^2/2\sigma_v^2\right] dv$$

$$= \frac{1}{2}\left[\operatorname{erf}\left(\frac{V_r - v_L}{\sigma_v \sqrt{2}}\right) + \operatorname{erf}\left(\frac{v_H - V_r}{\sigma_v \sqrt{2}}\right)\right] , \qquad (4.9)$$

where $V_r = V_r(r,\theta)$ is given in equation (4.7).

e) The Antenna Temperature

The antenna temperature is the convolution of the antenna pattern with the source function. In the preceding development, the source function is the product of the hydrogen distribution and the channel receptivity field. Hence the antenna temperature is

$$T_A(\xi_B,\eta_B) = \iint A(\rho)\ H(\rho,\phi)\ F(\rho,\phi)\ \rho d\rho d\phi \ , \qquad (4.10)$$

where $\rho d\rho d\phi$ is an element of area in the plane of the sky.

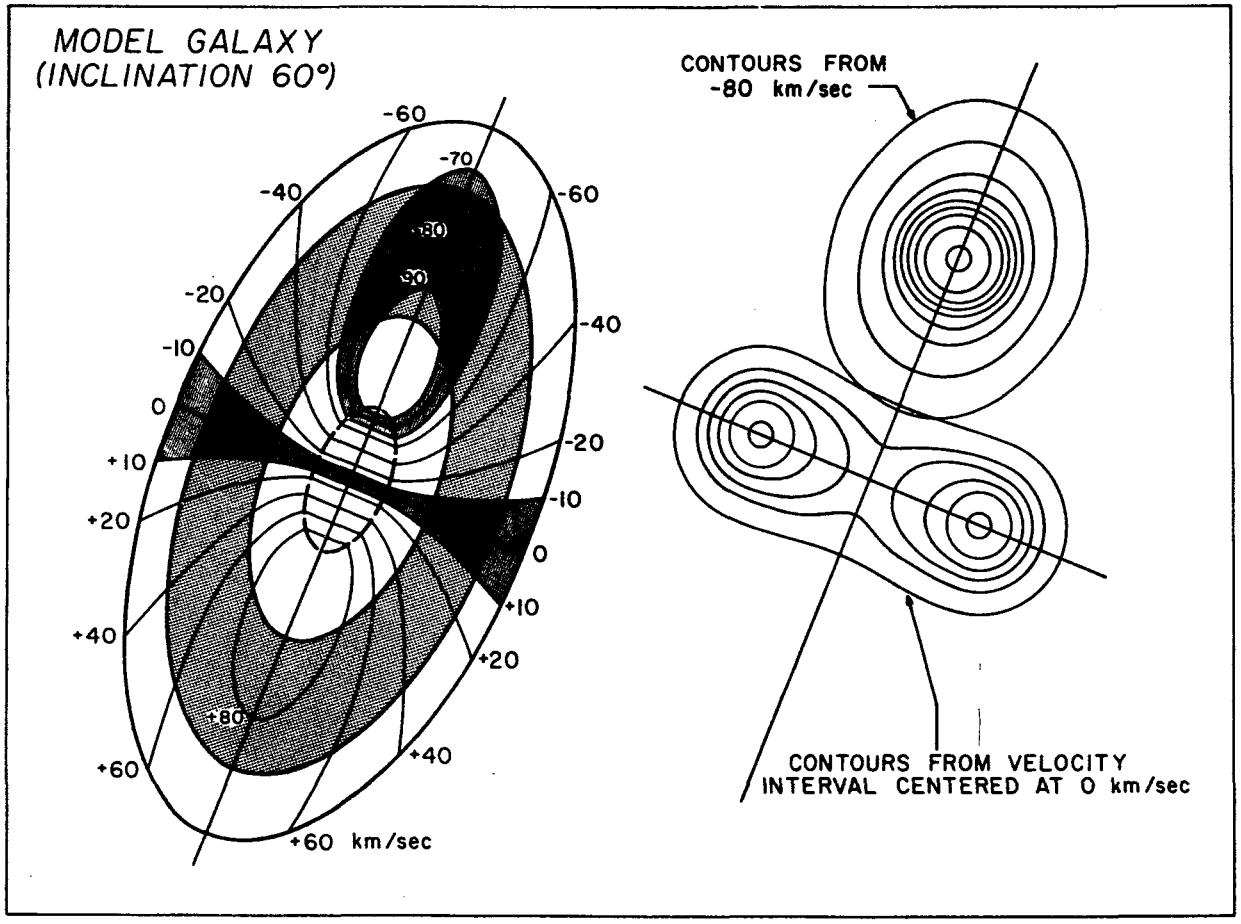


Figure 13. — A Model Galaxy in Pure Rotation. The stippled ellipse represents a ring of neutral hydrogen in the plane of the galaxy. The shaded regions depict the channel-receptivity field for channels centered at 0 and -80 km/sec. The contours represent the beam-smeared response of these two channels to the emission from the model galaxy.

However, it is advantageous in conformance with the preceding discussion to carry out the integration in the plane of the galaxy:

$$T_A(x_B,y_B) = \iint A(r,\theta)\ H(r)\ F(r,\theta)\ r dr d\theta. \qquad (4.11)$$

f) The Numerical Integration Algorithm

The plane of the sky is divided up for the purpose of numerical integration into a series of circular annuli concentric with the antenna beam. The diameter of the central disc and the width of the innermost annulus are taken to be

$$d\rho = \text{Min}\ [(30\ \text{km/sec})/A,\ \sigma_H,\ r_D,\ \tfrac{1}{4}\ \text{HPBW}].\ \sqrt{\epsilon}\ , \qquad (4.12)$$

where $A = 3^{3/2n}\ (V_m \csc i)/R_m$ is a measure of the maximum slope of the rotation curve,

σ_H is a measure of the width of the hydrogen ring,

r_D is the radius of the hydrogen disc,

HPBW is the half-power beamwidth of the antenna, and

ϵ is a measure of the desired fractional accuracy of the computation.

The area of the central disc in the plane of the galaxy is $(\pi/4)\ d\rho^2/\cos i$. The width of the m^{th} annulus is given by

$$h_m = d\rho\ \sqrt{A(\rho'_m)}, \qquad (4.13)$$

where $A(\rho'_m)$ is the antenna response at a distance ρ'_m and ρ'_m is the distance of the inner edge of the m^{th} annulus from the center of the beam.

The first annulus is divided into eight sectors; the m^{th} annulus into 4ν sectors:

$$\nu = (\pi/2)\ \rho_m/h_m\ , \tag{4.14}$$

where ρ_m is the distance from the beam center of the midpoint of the m^{th} annulus, and h_m is the width of the m^{th} annulus.

It can be seen from these considerations that the product of antenna response and the area (dS) of the integration element remains practically constant throughout the entire integration. The center of each area element is chosen as a representative point for that element. The positions of the area elements are determined by specifying that four representative points lie on the x and y axes, and the remainder be spaced uniformly in ϕ. The coordinates of the representative points are transformed from (ρ,ϕ) to (x,y) and the element of antenna temperature calculated.

$$dT_{mj} = A(\rho_m)\ H(x_{mj},y_{mj})\ F(x_{mj},y_{mj})\ dS_m \tag{4.15}$$

Summation takes place over all sectors in the m^{th} annulus. The integration continues until two conditions are simultaneously satisfied

$$\begin{aligned} &(1) \quad A(\rho_m) < \varepsilon \\ &(2) \quad \sum_j dT_{mj} \Big/ \sum_m \sum_j dT_{mj} < \varepsilon \end{aligned} \tag{4.16}$$

or, in words, the integration must proceed until reaching points of small antenna sensitivity and until the contribution to the antenna temperature

of the last annulus is less than a desired fraction of the total antenna temperature.

g) Comparison with Observed Data

After computing a model temperature for each point on the observed drift curve, the program normalizes the model drift curve and computes the r.m.s. of the point-by-point differences between the observations and the model predictions. Two different normalizations are used: one to the observed peak value of a drift curve (defined by the mean of the three highest points), and one to the area under the curve. When all drift curves have been processed, the program calculates the mean of the r.m.s.'s for the drift curves, and the r.m.s. scatter of the individual normalization factors about their mean. These two numbers for each type of normalization form quantitative criteria of the goodness of fit of the model to the observations.

The normalization to the peak of a drift curve provides an indication of the relative shapes of the observed and computed drift curves in that portion of the curves where the signal-to-noise ratio is highest. The normalization to the area under the drift curve fixes the amount of hydrogen measured by that drift curve. The scatter about the mean of the individual area normalization factors provides information on how well the model distributes the hydrogen among the various drift curves.

3. The Observations and the Models

a) Observational Data

Figure 14 contains contour maps of antenna temperature for eleven frequency intervals covering the range of radial velocities found in M33. These maps were constructed in the same manner as that in Figure 3, using

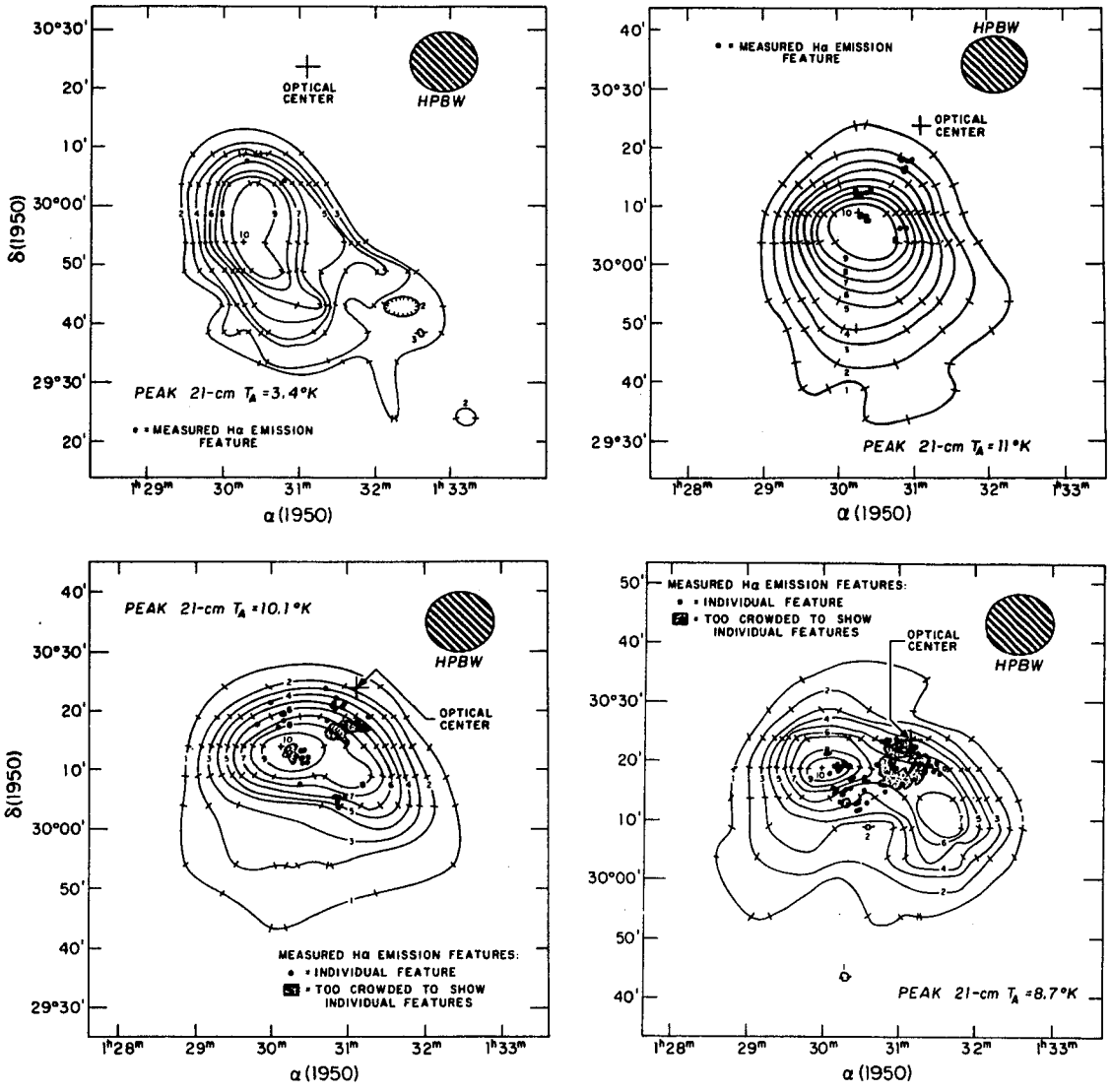


Figure 14(a-d). — Individual-Channel Contour Maps. These maps show the distribution of beam-averaged antenna temperature in each of the eleven channels covering the range of radial velocities in which 21-cm radiation from M33 was detected. The contours are drawn at intervals of 0.1 times the peak T_A in each map: thus the contour levels change from one map to the next. For comparison between the kinematics of neutral and ionized hydrogen, the data of Carranza et al. (1968) from Hα interferometry are included. The optical data are more nearly complete for the southern half of M33 than for the northern. The maps on this page cover the velocity intervals -70 to -91, -91 to -112, -113 to -134, and -134 to -155 km/sec.

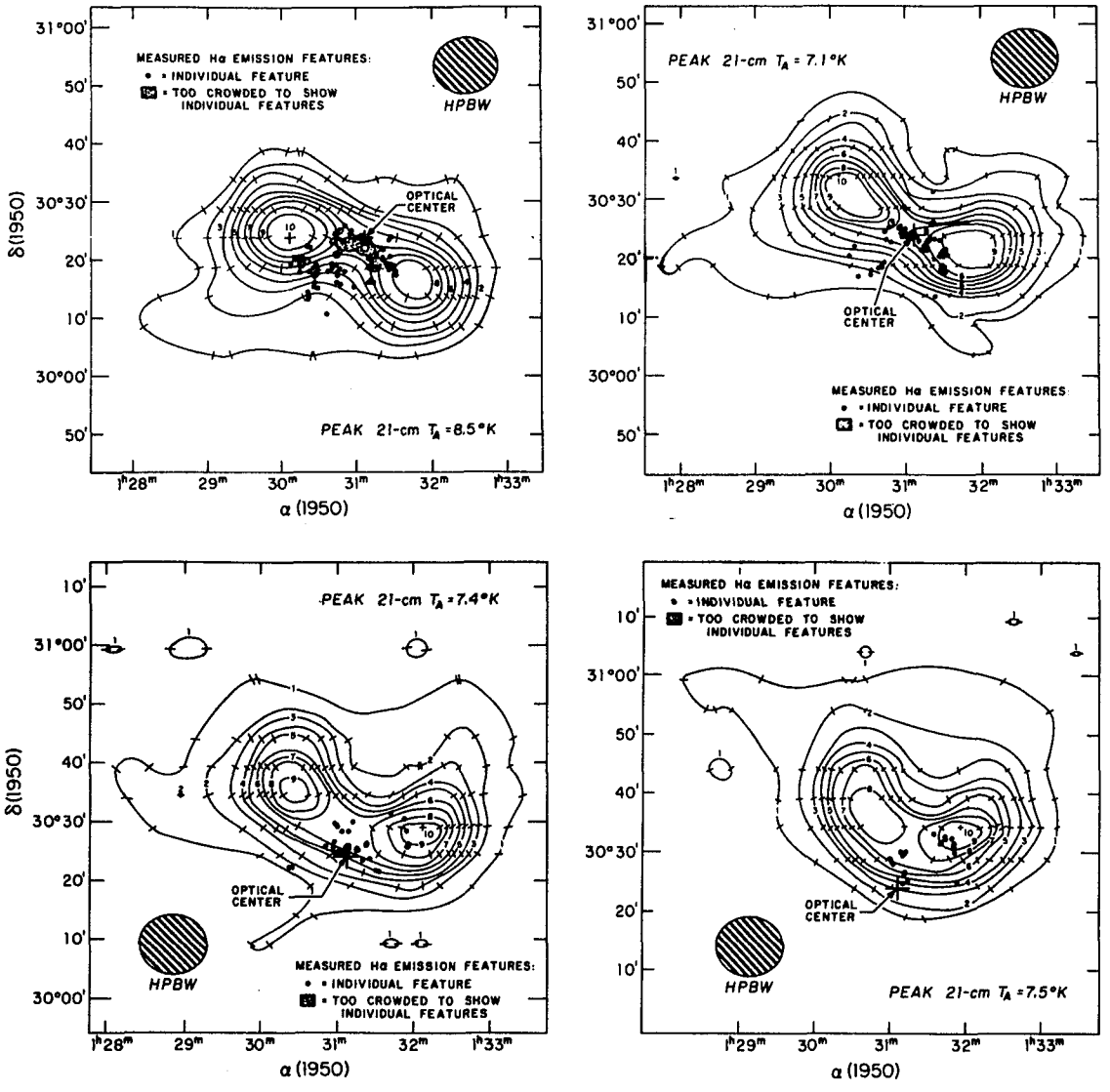


Figure 14(e-h). — Individual-Channel Contour Maps. The maps on this page cover the velocity intervals -155 to -176, -176 to -197, -197 to -218, and -218 to -239 km/sec.

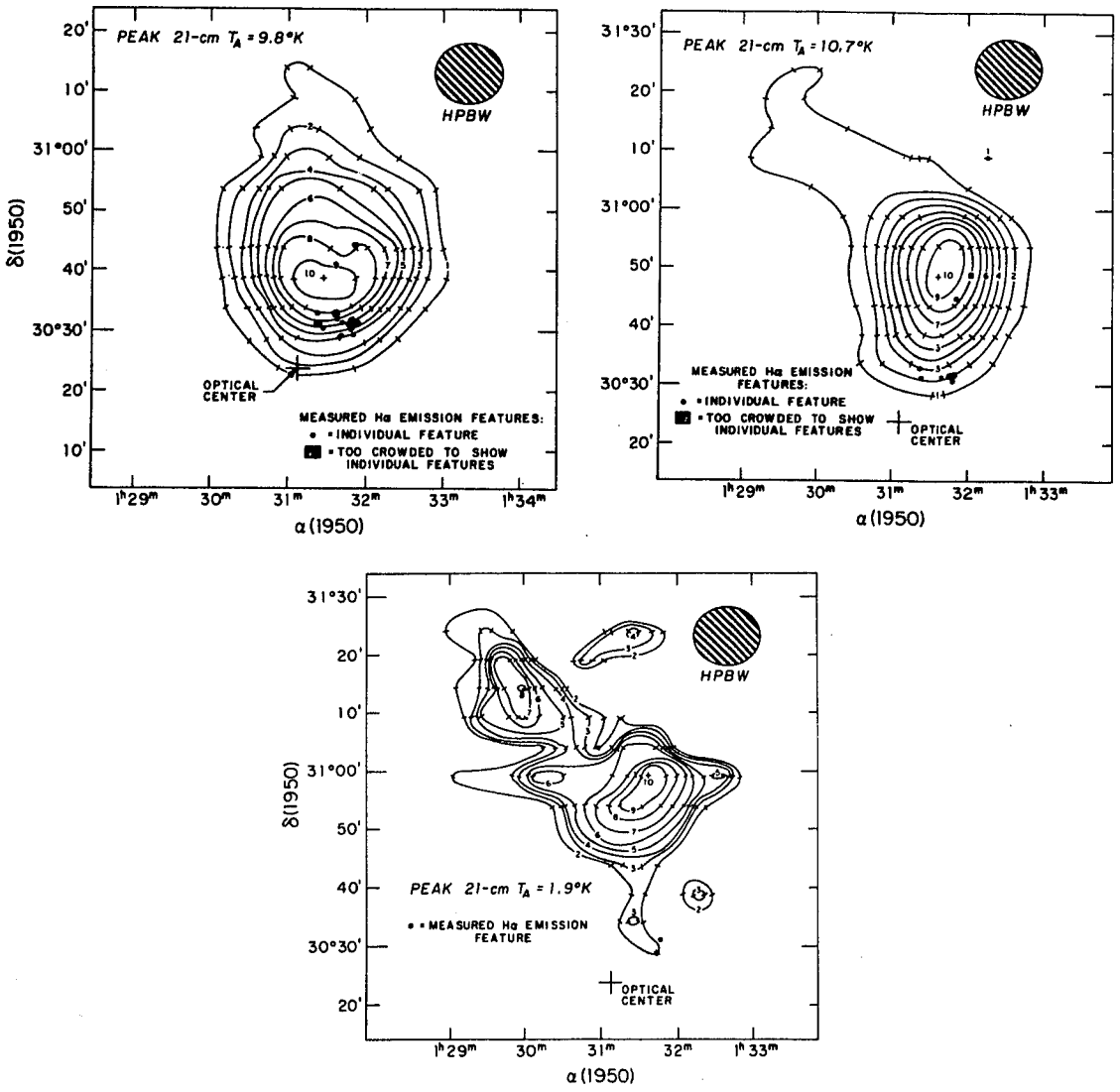


Figure 14(i-k). — Individual-Channel Contour Maps. The maps on this page cover the velocity intervals -239 to -260, -260 to -281, and -281 to -302 km/sec.

drift curves of individual channels. Because the channel centers for the scans 25' N and S of the center of M33 were offset by ∿7 km/sec (∿1/3 of a channel) from the channel centers at other declinations, the scans at these two declinations could not be used in the preparation of the contour maps.

These maps show a systematic positional displacement as a function of radial velocity, the maps for more negative radial velocities being centered progressively further north along the major axis of the galaxy. Also, the contours for channels near the systemic velocity are broadest in a direction parallel to the minor axis of the galaxy. From comparison with Figure 13 one may see that this is the expected behavior if the observed radial-velocity range is produced primarily by the rotation of the galaxy. Further evidence that circular motion is dominant over non-circular motions comes from the good agreement in position angle between the geometrical minor axis of the galaxy (112°) and its kinematical minor axis, defined by the lines connecting the peaks of double-peaked contours in Figure 14 (cf. Table 4). Radial motions in the galactic plane would produce a rotation of the kinematical minor axis with respect to the geometrical minor axis.

b) Hydrogen Distribution

Because the channel receptivity field for an individual channel forms a strip whose width increases with increasing distance from the galactic center (see Fig. 13), the contour map of antenna temperature for an individual channel near the systemic velocity will display a slight central depression even if the surface density of neutral hydrogen is uniform throughout the galaxy. However, the central depressions

TABLE 4

PEAKS OF SINGLE-CHANNEL CONTOUR MAPS

Channel V_r [km/sec]	Peak Position $\Delta\alpha$	$\Delta\delta$	Peak-to-Peak separation	p.a.
- 81	- 9!3	-25!9		
-102	- 9.7	-18.4		
-123	-11.2	-10.6	10!7	111°
	- 1.3	-14.4		
-144	-14.4	- 5.1	20.6	111
	+ 5.2	-12.5		
-165	-12.5	+ 1.3	22.6	112
	+ 8.4	- 7.2		
-186	-10.8	+ 7.5	22.7	115
	+ 9.9	- 2.1		
-207	- 9.1	+11.3	22.9	110
	+12.9	+ 4.1		
-228	- 3.9	+12.5	14.6	104
	+10.6	+ 9.1		
-249	+ 4.5	+14.9		
-270	+ 8.0	+26.2		
-291	+ 6.7	+32.8		

in the maps in Figure 14 (see also Fig. 4) are quite pronounced. (The antenna temperatures at the saddle points in Figure 14e,f are ∿65% of the peak temperatures.) Therefore there must indeed be a lack of hydrogen in the central regions of M33, compared to the amount found at distances of 15'-20' from the center. Figure 15 contains contour maps for one channel of model galaxies with a ring of hydrogen, with uniform hydrogen, and with a centrally condensed hydrogen distribution. These maps may be compared with panel (f) of Figure 14, which contains the observed contours for the same radial-velocity interval. The model parameters adopted as representing the hydrogen distribution in M33

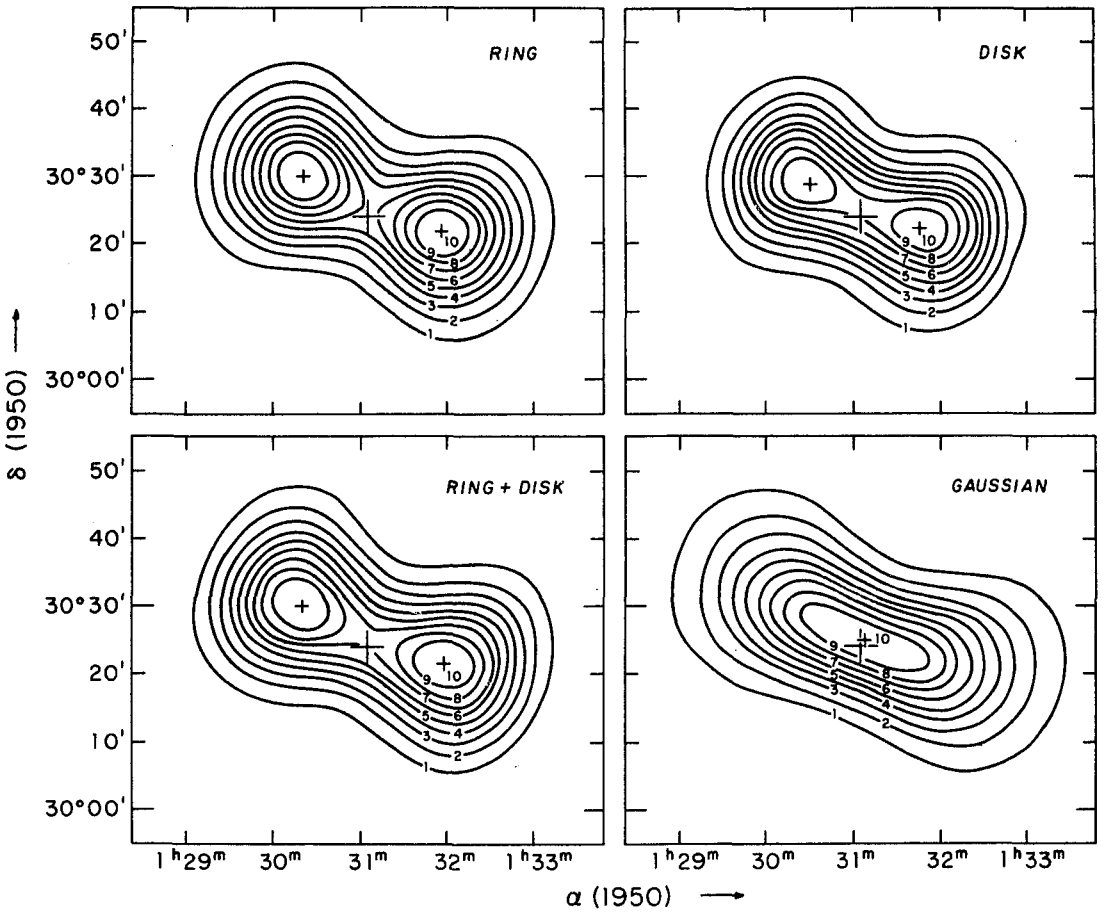


Figure 15. — Model-Galaxy Contour Maps. The maps on this page cover the velocity interval -176 to -197 km/sec, and may thus be compared with the observational data in Fig. 14(f). The model galaxies used in the construction of these maps had identical rotation-curve parameters, but different parameters for the distribution of neutral hydrogen.

were derived from comparison with the integrated H I contours (Fig. 3) and with the two individual channels nearest the systemic velocity (Fig. 14e,f). The adopted parameters refer to the main body of the galaxy, because of the assumption of circular symmetry. In particular, the np and sf wings were ignored in the fitting. Table 5 contains the adopted values of the H I distribution parameters.

TABLE 5

ADOPTED VALUES FOR H I DISTRIBUTION PARAMETERS

Parameter		Value	
r_o	ring radius	18'	3.9 kpc
σ_H	ring thickness	10'	2.2 kpc
r_D	disk radius	35'	7.6 kpc
P	fraction of H I associated with ring	.33	
Maximum relative density ring/disk (H_o/H_D)		.66	

c) Inclination

In order to achieve a fit for the hydrogen distribution, one additional parameter has to be considered: the inclination i. The adopted value of 55° is compared in Table 6 with optical determinations by previous authors. Three of the values were derived from major and minor axis diameters of M33. Patterson derived her value from fitting ellipses by eye to isophotal contours at 30° intervals of position angle. The present value was determined from comparison of observed and computed integrated-H I contours, with greatest weight given to the contours near the half-maximum level. The optical values for the

TABLE 6

DETERMINATIONS OF THE INCLINATION OF M33

Author	b/a	i(0.0)	i(0.2)
Roberts (1899)	.57	56°	57°
Patterson (1940)	(.50)	60°	(62°)
Holmberg (1950)	.64	50°	52°
de Vaucouleurs (1959)	.62	52°	54°
Gordon (present paper)		55°	

inclination are listed both for the thin-disk assumption (c/a = 0) and for a finite axial ratio (c/a = 0.2). The latter values should be compared with the value derived from the distribution of neutral hydrogen, because the neutral hydrogen probably has a much flatter distribution than does the luminous matter in the galaxy (cf. §IV.1).

d) Systemic Velocity

Table 7A lists the values for the systemic velocity of M33 obtained by previous authors. Most of these refer to the value at the optical center of the galaxy. Some, on the other hand, were derived from the assumption of a symmetrical rotation curve or, equivalently, from the midpoint of the global velocity profile. Burke, Turner, and Tuve (1963) presented values obtained by both methods. They found a difference of 5 km/sec between the two, which they stated "is significant but is not understood." In the present study the systemic velocity was derived by five different methods, subject to the assumption that the rotational center of M33 coincides with its optical center.

(1) The placement in the sky of the contours for the two channels nearest the systemic velocity was compared between models and observations.

TABLE 7

THE SYSTEMIC VELOCITY OF M33

A. Previous Investigations

Author	S [km/sec]
Pease (1916)	- 70
Hubble (1936)	-320
Mayall and Aller (1942)	-167± 5 p.e.
Humason, Mayall, and Sandage (1956)	-189±15 est.
Volders (1959)	-175± 2
Dieter (1962)	-186± 5
Burke, Turner, and Tuve (1963)	-179± 1 (minor axis) -184 (major axis)
Brandt (1965)	-195± 7 p.e.
Meng and Kraus (1966)	-169
Davies (1967)	-179
Carranza, Courtès, Georgelin, Monnet, and Pourcelot (1968)	-172.5

B. Present Study

Method	S[km/sec]
(1) Single-channel contours	-178
(2) Minor-axis velocity profiles	-177
(3) Velocity profiles, central major axis	-183
(4) Symmetrical rotation curve	-183
(5) Best rotation curve, northern major axis	-180
" southern major axis	-180
Adopted	-180±2.5 (internal m.e.)*

* External error amounts to 7 km/sec per minute of arc pointing inaccuracy. An estimated mean pointing error of 20" in each coordinate, plus 20" for the optical position, yields an estimated external mean error of ± 4 km/sec.

(2) The quality of the model fits was evaluated, using the criteria outlined in §IV.2.g), for velocity profiles at points along the minor axis of M33. (3) The best-fitting model was found for velocity profiles in the central section of the major axis (between 10' N and 10' S of the galactic center); (4) for velocity profiles along the entire major axis, assuming a symmetrical rotation curve; and (5) for velocity profiles along the northern and southern halves of the major axis, without assuming a symmetrical rotation curve. The results are listed in Table 7B. The agreement between methods (2) and (4) and the corresponding values from the study by Burke et al. is quite satisfying. Although the differences between the values found using the five different methods may be real, they are not significant, since the filters used in this study were 20 km/sec wide. In addition to the internal uncertainty in the adopted value of -180 km/sec, there are external uncertainties introduced by the limited accuracy of the optical position of M33 and the pointing accuracy of the 300-ft telescope. The estimated mean error from both internal and external sources is $\pm$ 5 km/sec.

e) The Rotation Curve and the Total Mass of M33

From the factors sin θ and cos θ in equation (4.7), one can see that observations along the minor axis of a galaxy yield no hold on the rotation curve, while observations along the major axis yield the rotation curve uncontaminated by effects of expansion or contraction in the plane of the galaxy. Observations at other position angles contain the effects of both circular and radial motions. Model-galaxy velocity profiles were fit to profiles chosen along the major and minor axes, and at eight other position angles spaced at 30° intervals on the plane of the sky.

Table 8 contains the rotation-curve parameters determined from velocity profiles along the two halves of the major axis ($-38' \leq x \leq +43'$). The shapes of the two halves of the rotation curve are quite similar, but the amplitudes differ by 5 km/sec in radial velocity, or 6 km/sec in circular velocity, at maximum. This amount is significant with regard to the internal accuracy of the model-fitting procedure, and it could indicate that the rotational center of the galaxy lies slightly to the north of the optical center. Alternatively, it could indicate an asymmetrical mass distribution or the presence of asymmetrically distributed forces of nongravitational nature (e.g., magnetic fields) or large-scale motions perpendicular to the galactic plane. The indicated amount of the displacement is, however, only a fraction of a minute of arc and thus within the uncertainty of measurement of the relative optical and radio positions. On the other hand, placing the rotational center at the apparent centers of the H I and star-count distributions (which are south of the optical center) would increase the asymmetry of the rotation curve considerably. The low value of the shape parameter $n \sim 1$--by contrast, the Bottlinger (1933) rotation law sets $n = 3$--indicates a steep rise of the rotation curve and a broad plateau region.

Values of the rotation-curve parameters outside the permissible ranges yielded fits in which the r.m.s. deviation of the model points from the observations was at least 10% greater than for the best value. The quoted ranges are based on varying a single parameter while holding all others constant. However, it is possible to compensate partially a change in one parameter by an appropriate change in another: e.g., to decrease V_m and either increase σ_v or adjust S. In particular, the

TABLE 8

PARAMETERS OF THE ROTATION CURVE

Parameter	Northern Half Best Value	Northern Half Permissible Range	Southern Half Best Value	Southern Half Permissible Range
S	-180 km/sec	-182- -178	-180 km/sec	-182- -178
V_m	87 km/sec	85-89	82 km/sec	80-84
R_m	29'	26-32	30'	26-34
n	1.0	0.8-1.3	1.1	0.9-1.4
σ_v	12 km/sec	9-14	13 km/sec	11-15
$M_t/M_\odot$	5.4×10^{10}	3.5-8.4	4.4×10^{10}	2.9-6.7

compensating effects of simultaneously adjusting V_m and S produced a very broad range of acceptable fits for the major-axis velocity profiles. The magnitude of the asymmetry in the rotation curve is therefore critically dependent upon the value of the systemic velocity. From the results of methods (1) and (2) in §d) and from the model fitting described in §f), one may conclude that the asymmetry may be a few km/sec larger than quoted in Table 8, but that it is unlikely to be smaller.

An infinitesimally thin galaxy with a rotation curve of the form of equation (4.4) has a total mass (Brandt 1960) of

$$M_t = A^2/B^3G \ , \tag{4.17}$$

where G is the gravitational constant. Using the parameters of equation (4.5), one obtains

$$M_t/M_\odot = 6.77 \times 10^4 (1.5)^{3/n} R_m D V_m^2 \operatorname{cosec}^2 i \ , \tag{4.18}$$

where D is the distance to the galaxy in megaparsecs. Masses corresponding to values of D = 0.72 Mpc, i = 55°, and the rotation-curve parameters in Table 8 are listed in the last line of the table.

Table 9 compares an average mass for the galaxy with the masses derived in studies by previous investigators. The published values were corrected for differences in the assumed inclination of and distance to M33 and, where necessary, for the assumption of an infinitesimal axial ratio. Brandt (1960) has shown, for the inner parts of a galaxy with a given rotation curve, that the mass is approximately proportional to $1 + c/a$. For an Sc galaxy like M33, an axial ratio of $c/a = 0.1$ is probably appropriate. Strictly, this correction factor must be a function of radius and must approach unity as $r \to \infty$. The data used by many of the previous authors extend over only a portion of the area covered by our measurements. In addition, the models in some of these studies are terminated at still smaller radii. Hence, the comparisons are made with the mass of the present model contained within a cylinder of the appropriate radius. The values of the mass fraction used in the computation of the truncated masses were taken from the table published by Brandt and Scheer (1965).

If one restricts one's view to values of the mass contained within a cylinder defined by the limit of the data, one finds agreement within a factor of two between the present study and all previous studies. This discrepancy can easily be accounted for within the measurement error. The values for the total mass, however, range by an order of magnitude. (Note that the 10% correction for finite axial ratio was not applied to these values.) These values are all based upon extrapolations beyond the data under the assumption of a particular shape of the rotation curve. The present observations cover a larger portion of the rotation curve with greater resolution than do any of the previous surveys, including the one by Brandt (1965) in which all of the data beyond the

TABLE 9

THE TOTAL MASS OF M33

Reference	Assumed Distance [kpc]	Assumed c/a	Assumed Inclination	Limiting Radius	Masses [10^{10} $M_\odot$] Published	Corrected	Comparison
Wyse and Mayall (1942)	220	0	57°	17!5	0.17	0.64	0.76
				30	0.20	0.75	1.4
Aller (1942a)	220	0	57	16	0.18	0.68	0.70
Schwarzschild (1954)	480	0	57	40	0.50	0.86	1.7
Lohmann (1954)	440	0	57	30	0.72	1.4	1.4
				∞	1.0	1.7	4.9
Kerr and de Vaucouleurs (1956)	440	0.1	57	40	0.55	0.94	1.7
Takase (1957)	540	0.08	57	19	0.40	0.57	0.86
				∞	0.44	0.61	4.9
Volders (1959)	630	small	57	45	1.8	2.2	1.9
Dieter (1962)	630	0	57	60	1.2	1.6	2.3
Brandt (1965)	630	0.1	57	60	1.8	2.2	2.3
				∞	3.4	3.7	4.9
Takase and Kinoshita (1967)	630	0	57	41.5	0.64	0.84	1.8
				52	0.69	0.91	2.1
				∞	0.77	0.92	4.9
Gordon (present paper)	720	0.1	55	∞	4.9		

peak of the rotation curve originated from the studies by Volders (1959) and Dieter (1962) with half-power beamwidths of 34' and 53', respectively. Within the framework of the assumed family of rotation curves, therefore, the present data should more accurately define the shape of the curve than did any of the previous observations. One may legitimately question whether equation (4.5) adequately represents the rotation curve of the galaxy--since it predicts that less than half of the total mass of M33 is contained within the limit of the data, and this fraction increases quite slowly with increasing radius. But it is doubtful that this question could be decided on the basis of the present data.

f) Comparison of the Distributions of Mass, Light, and Neutral Hydrogen

The form of the rotation curve and the projected surface distribution of mass in a galaxy are uniquely related. Brandt and Scheer (1965) have tabulated dimensionless surface densities for rotation curves of the form of equation (4.5). The values for the mass surface density of M33 are tabulated in the second column of Table 10 as a function of radius. The surface brightnesses in the third column are derived from the B photometry by de Vaucouleurs (1959). Characteristic radii were obtained from the areas contained within given isophotes. The effects of inclination were removed by use of the average apparent axial ratio $\langle b/a \rangle = 0.615$. The conversion to solar units is based upon an apparent blue distance modulus of 24.6 (de Vaucouleurs 1966) and an absolute solar magnitude of +5.47 (Stebbins and Kron 1957). A similar procedure applied to the contours in Figure 3 yields the surface densities of neutral atomic hydrogen in the fourth column. In this case an inclination of 55° was assumed in correcting the calibration of equation (3.1).

TABLE 10

COMPARISON OF THE DISTRIBUTIONS OF MASS, LIGHT, AND NEUTRAL HYDROGEN

r [']	Σ_t $[M_\odot/pc^2]$	Σ_B $[L_\odot/pc^2]$	Σ_{HI} $[M_\odot/pc^2]$	Σ_t/Σ_B $[M_\odot/L_\odot]$	Σ_{HI}/Σ_B $[M_\odot/L_\odot]$	Σ_{HI}/Σ_t
5	275	111	8.5	2.5	0.077	.031
10	180	54	8.3	3.3	0.154	.046
15	130	30.5	7.9	4.2	0.26	.062
20	85	17.3	7.4	4.9	0.43	.087
25	73	9.5	6.7	7.7	0.71	.092
30	48	4.5	5.1	10.7	1.13	.106
35	36	2.0	3.5	18	1.8	.097
40	29	0.9:	2.1	30:	2:	.073
50	19	0.1:	0.9	150:	7:	.046

The ratios in the last three columns of the table show that both the total-mass and light distributions are centrally peaked, but the distribution of neutral hydrogen is not. In the outer part of the galaxy, the distribution of hydrogen and total mass are more nearly proportional to each other than either is to the distribution of blue light. Both the hydrogen and total-mass distributions are more extended than is the light. This could be interpreted as support for the hypothesis that the formation of stars, and particularly of highly luminous stars, depends on a power greater than one of the density of matter.

g) Departures from Circular Motion

Because all velocity profiles within each group used in the fitting program lie along a single radius vector in M33 [see §e)], the fitting is free of any assumptions regarding the dependence of noncircular motions on position angle (θ). These motions may manifest themselves to the

fitting program either by requiring different rotation curves for each set of velocity profiles or by requiring non-zero values for the expansion parameters in equation (4.7). In either case, the program is actually fitting the magnitude of the line-of-sight component of the non-circular velocity as a function of r. This component may contain contributions from motions along a radius vector in the plane of the galaxy (expansion/contraction), or motions perpendicular to the galactic plane, or both.

Table 11 contains the results of the model fitting for the several position angles. In the last two columns of the table the departures from circular motion are expressed respectively as the change in maximum velocity of the rotation curve from the values in Table 8 (ΔV_m) and as the amplitude of expansion in the galactic plane (E_o). With two exceptions, the basic rotation curves fit the data with an r.m.s. inside the acceptable range of 10% above the best fit. One of the exceptions (p.a. 352°)

TABLE 11

MODEL FITTING FOR VELOCITY PROFILES OFF THE MAJOR AXIS

Position angle	No. of profiles	Basic rotation curve	ΔV_m [km/sec]	$E_o(\kappa = 3)$ [10^{-4}(km/sec)/min arc^3]
52°	7	N	-9 ± 4	$+12\pm4$
82-262	8	N	-7 ± 5	$+2\pm3$
		S	-1 ± 7	$+0.5\pm2.5$
112-292	7	-	-	0 ± 2
142	5	S	$+3\pm6$	$+2\pm2$
172	7	S	$+1\pm3$	$+2\pm4$
232	5	S	$+3\pm3$	-3 ± 3.5
322	7	N	-2 ± 6	-2 ± 2
352	10	N	$+3\pm3$	$+5\pm4$

is only marginally outside the permissible range. Different values of $\kappa > 0$ produced very little difference in the quality of the fits achieved. Values of $\kappa < 0$ did not produce acceptable fits. Although the parameter values in the table refer to sets of models in which the systemic velocity was taken to be -180 km/sec, better fits were obtained for the minor-axis profiles with S = -177 km/sec and for the other groups with S = -178 or -179 km/sec. Again, the differences in fit were at most marginally significant. However, the trend of S with position angle [already noted in §d) and by Burke et al. (1963)], together with the results of Table 10, probably indicate that there are noncircular motions of several km/sec in M33 with a more complex positional dependence than can be handled by the equations used in the model-fitting analysis.

h) Comparison of the Kinematics of Neutral and Ionized Hydrogen

The general agreement between the kinematics of neutral and ionized hydrogen in M33 can be seen in Figure 14, which contains, in addition to the H I contours for individual channels, the data of Carranza et al. (1968) in the corresponding velocity intervals. The optical points fall, on the whole, in a band between the peaks of the radio contours. They conform to the pattern, shown in Figure 13, of a smaller optical distribution and a larger 21-cm distribution delineating the inner and outer portions, respectively, of the same radial-velocity loci.

Carranza et al. have noted an asymmetry in the rotation curve in M33, in the same sense as described in §e), but of greater magnitude. Much of the discrepancy in magnitude can be accounted for by the different values chosen for S (-172.5 vs. -180 km/sec). They also found that gas in the spiral arms appeared to follow a different rotation law than gas between the arms. This may explain the indications for noncircular

motion found in §g). The group of 21-cm velocity profiles with the strongest indication of noncircular motion is the group containing profiles of NGC 604. Scans obtained at the declination of NGC 604 with the 100-channel autocorrelation receiver (velocity resolution ∿2 km/sec) indicate the presence of a concentration of neutral hydrogen at the position of NGC 604 with a radial velocity of ∿-245 km/sec (approximately 20 km/sec negative of the main peak of the velocity profile). The velocity width for the feature cannot be determined from the present data, since it occurs on the shoulder of the main peak. The optical measurements of the velocity of NGC 604 show a wide range: the mean of four plates from the study by Mayall and Aller (1942) differs by 45 km/sec from the mean of two plates by Brandt (1965). The observations of Carranza et al. indicate internal motions in the region with a range of 50 km/sec, encompassing the other optical values and centered around -255 km/sec.

i) Kinematics of the Outermost Parts of the Galaxy

As noted above, the adopted parameters of the neutral-hydrogen distribution refer to the main body ($r \lesssim 9$ kpc) of the galaxy. Beyond this radius, the surface density of neutral hydrogen appears to decrease more slowly than predicted--particularly in the position angles at which the "wings" are encountered. Velocity profiles from the outermost portions of M33 were therefore excluded from the model fitting described in the previous sections. Most of the signals from these outer regions are weak. There are, however, signals in these regions which are strong enough to invite at least semi-quantitative analysis.

Figures 16 and 17 depict the velocity field in M33, uncorrected for the effects of beam smearing. They are analogous to the drawing in the left half of Figure 13, which represents a model galaxy in pure rotation.

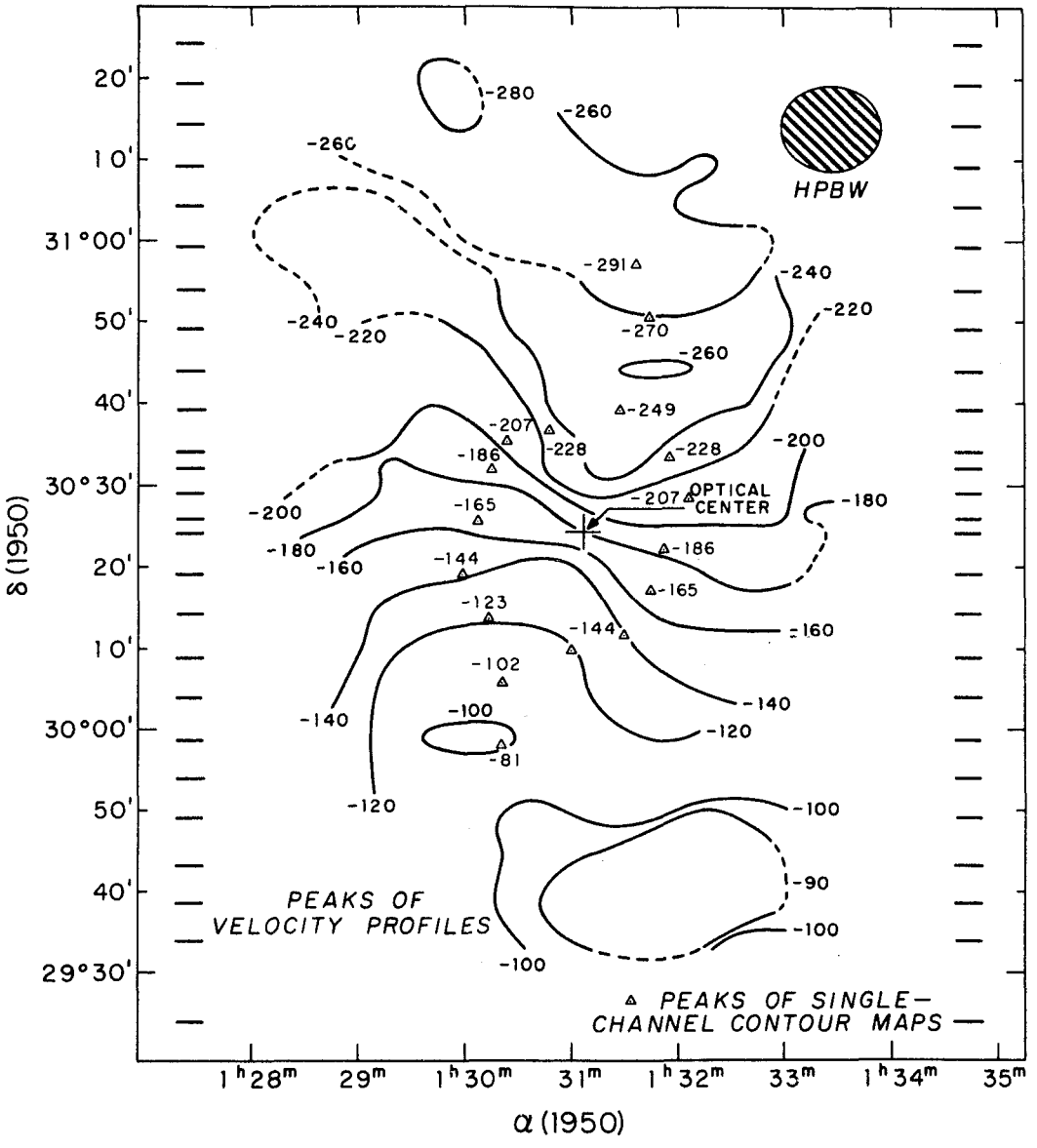


Figure 16. — Radial-Velocity Loci. The isovels in this figure depict the radial-velocity field in M33, uncorrected for the effects of beam smearing. The loci were derived from the peaks of velocity profiles every 10^s in right ascension at the declinations indicated by the horizontal bars along both sides of the map. Dashed lines indicate portions of the loci which are uncertain because of poor signal-to-noise ratio. The triangles locate the peaks of the contour maps in Fig.14.

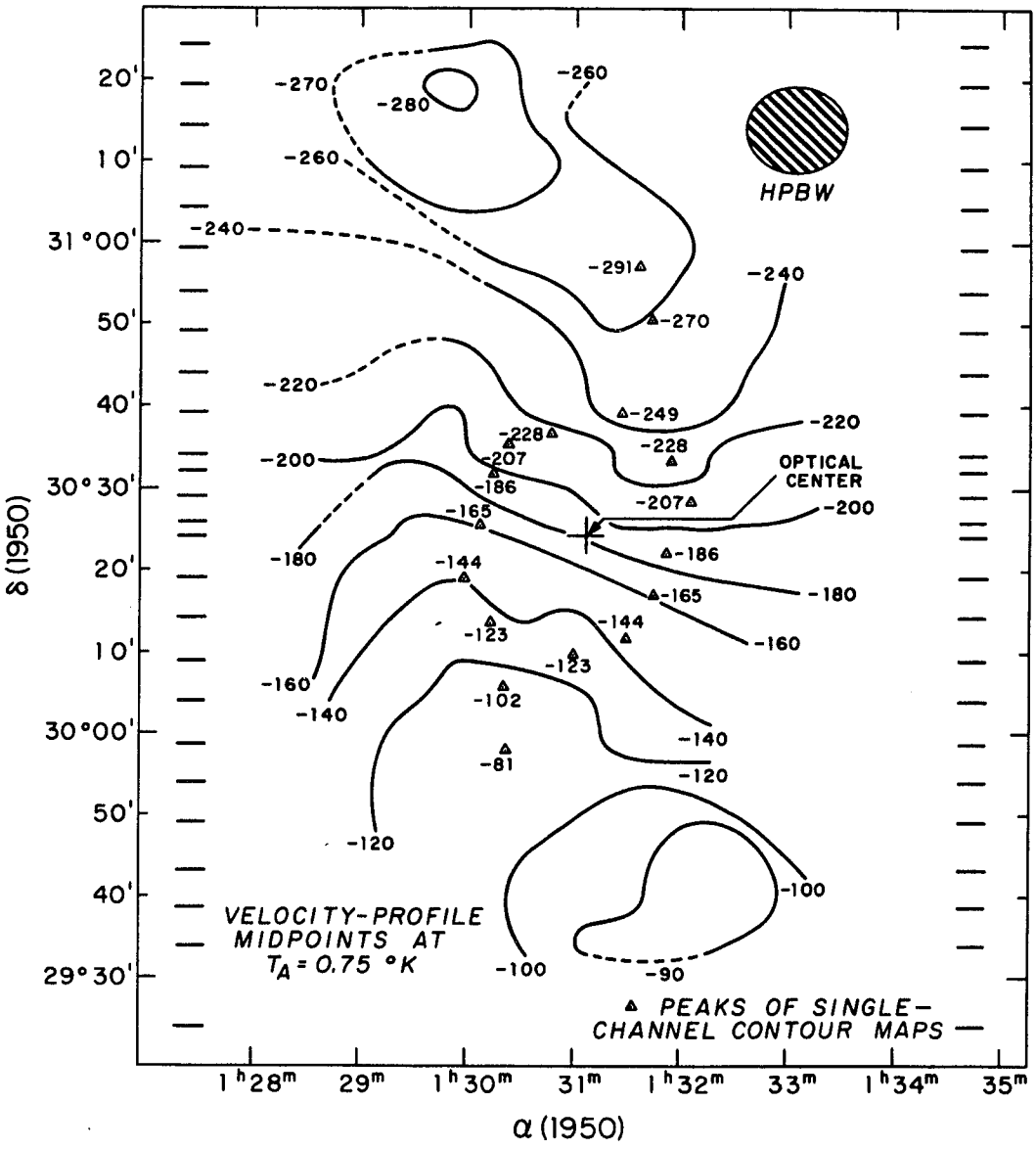


Figure 17. — Radial-Velocity Loci. The isovels in this figure were constructed from the midpoints of velocity profiles rather than their peaks. Otherwise the remarks of the caption to Fig. 16 apply.

Figure 16 is constructed from the peaks of velocity profiles recorded at intervals of 10^s along each drift curve. Figure 17 is constructed from the same velocity profiles, but is based on the velocities midway between the points at which the profiles reach an antenna temperature of $T_A = 0.75°$ K. This level was chosen to lie safely above the r.m.s. noise and yet include profiles at large distances from the center of the galaxy. The differences between these two diagrams can be ascribed totally to the effects of beam smearing. (One clear difference is in the spacing of the isovels near the galactic center.) The contours in Figure 18 show how the widths of the velocity profiles decrease with increasing distance from the center of M33. This effect reflects both the increasing spacing between the isovels and the weakening of the signals from the outer parts of the galaxy. The former phenomenon dominates within $r \sim 6$ kpc, while the latter phenomenon controls the appearance of the lowest contours.

Two local extrema can be seen in Figure 16 on the major axis of M33, near the positions of the peaks of the rotation curve. But the real extremes of the velocity field, in both figures, occur further out from the center of M33 and well away from the major axis. The outer ends of all the isovels are bent in the same direction as these extrema are displaced from the major axis. The gas which is at these extreme radial velocities cannot be traveling in circular orbits in the galactic plane.

If one assumes that all gas in M33 is situated in the galactic plane, then the displacement of the velocity extrema from the major axis is a result of expansion. The model-fitting approach was applied to ten velocity profiles in the np wing and to seven in the sf wing. On the basis of the rotation-curve parameters in Table 8, these velocity profiles require the expansion parameters in Table 12. The first two lines of the

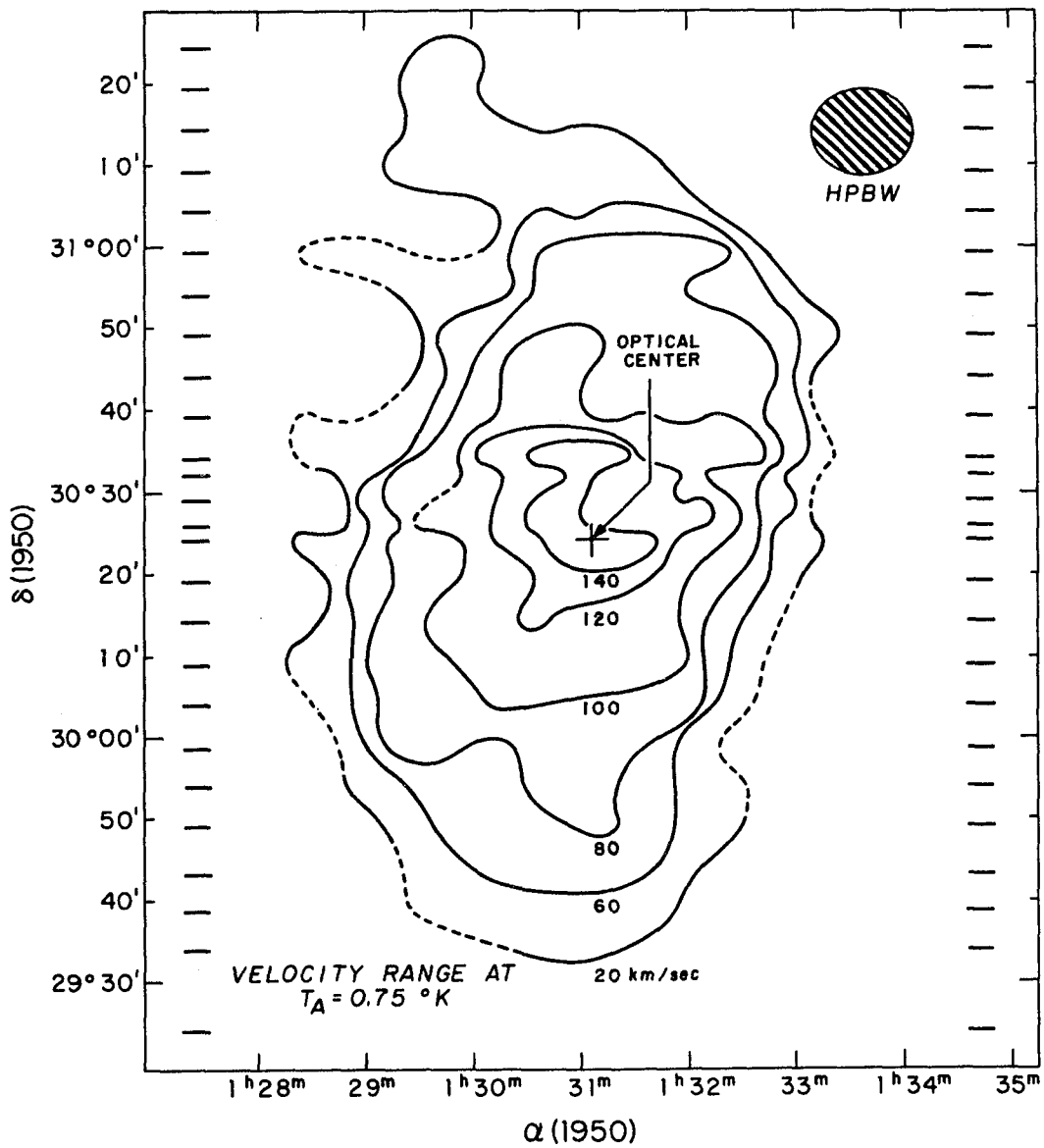


Figure 18. — Radial-Velocity Range. This contour map shows the width of the 21-cm velocity profiles at the same level of antenna temperature as was used in creating the map of the velocity field in Fig. 17.

TABLE 12

MODEL FITTING FOR VELOCITY PROFILES IN THE WINGS

Parameter	North-Preceding Wing		South-Following Wing	
	Best Value	Permissible Range	Best Value	Permissible Range
κ	1	0 - 2	-0.5	-1.5 - +0.5
E_o[(km/sec)/(min arc)$^\kappa$]	1.05	0.9 - 1.2	500	425 - 575
R[']	70		55	
$E_o R^\kappa$[km/sec]	74	64 - 84	67	57 - 77
ΔV_r[km/sec]	-48	-41 - -55	40	34 - 46
Z_o[km/sec]	88	75 - 101	73	62 - 84
K_z[10^{-10} cm/sec^2]	8.9		13.6	
z_m[kpc]	14.3	10.5-18.8	6.6	4.8 - 8.7

table contain the values of the parameters of equation (4.7). In the next two lines, the solutions are expressed as actual expansion velocities at representative galactocentric distances in the wings. In the fifth line of the table, the trigonometric factors have been removed to show the observed deviation of the radial velocity in the wings from the radial velocity predicted by the rotation curve. The derived expansion velocities are ∿70 km/sec, an order of magnitude larger than those found in the main body of the galaxy, and there is an indication (at least in the np wing) that the expansion velocity is still increasing outward. Both of these factors would have to be explained before this model of the kinematics could be accepted.

The model discussed above has dealt purely with the kinematics. However, one must also note that the wings contain significant amounts of neutral-hydrogen gas--since they are visible in the integrated H I contours

of Figure 3. Planimetry of this figure, including a contour below the lowest one shown, yields estimates of 1.0 x 10^8 $M_\odot$ of hydrogen in the np wing and 0.5 x 10^8 $M_\odot$ in the sf wing. The integrated surface density is 5-10 times larger in the wings than at similar distances from the center at other position angles. These numbers are quite uncertain because of the difficulty of separating the wings from the main body of the galaxy.

There are three basic ways in which one might explain the difference in surface density as a function of position angle while maintaining the concept of a layer of neutral hydrogen comprising a galactic plane: either by a difference in space density, or by a difference in the thickness of the hydrogen layer, or by a warp in the layer producing a difference in the line-of-sight distance through it.

In order to produce an effect of the observed magnitude, the warp would have to change the effective inclination of the galactic plane from 55° to 85°. The increased inclination would account for about 15 km/sec of the observed ΔV_r (cf. Table 12) as projected circular velocity. However, most of the remainder would still have to be explained as expansion, since motions perpendicular to the galactic plane would also be very nearly perpendicular to the line of sight. The warp would produce a "hatbrim" effect in M33 with a semi-amplitude of 7 kpc at r = 12 kpc (= 57' along the major axis), if one assumes that the "hatbrim" has a form $z(r,\theta) = A(r) \sin (\theta-\theta_o)$, and the amplitude A(r) is chosen to produce a maximum tilt of 30° with respect to the mean plane of the galaxy. By contrast, the "hatbrim" observed in the outer part of the Milky Way Galaxy reaches a height of 900 pc above the plane (along a diameter perpendicular to the sun-center line) at r = 15 kpc, the largest distance for which both northern and southern data are available (Kerr

1969). On the northern side, with the larger warp, the "hatbrim" reaches a height of 1600 pc at r = 16 kpc.

In attempting to account for a possible hatbrim in M33, one may compare the tidal force exerted on M33 by M31 to that exerted on the Milky Way by the Magellanic Clouds. Using the data compiled by Roberts (1968b), one finds that M31 is 26 times as massive as the Clouds (31 vs. 1.2 x 10^{10} $M_{\odot}$) but 3.3 times as far away from M33 (190 kpc) as the Clouds are from the Galaxy (57 kpc). Since tidal forces vary inversely as the cube of the distance, the tidal attraction of M31 for M33 is only 0.7 times that of the Magellanic Clouds for the Milky Way. To complete the analogy, and calculate the expected relative heights of the hatbrims, one should know the relative surface densities of matter in the plane of M33 at 12 kpc from its center and in the plane of the Galaxy around 17 kpc from its center. Brandt and Scheer (1965) have tabulated the necessary functions for computing surface density from rotation-curve parameters. For M33 one can use the parameter values in Table 8, and for the Milky Way V_m = 255 km/sec, R_m = 8.66 kpc, n = 3: these values represent the Kwee, Muller, and Westerhout rotation curve scaled to the presently accepted value of $R_{\odot}$ = 10 kpc (Shane and Smith 1966), and produce a solar-neighborhood value of K_z which is in good agreement with the value cited by Oort (1965). The surface density of our Galaxy at R = 17 kpc is 7.4×10^{-3} g/cm^2, or 2.8 times the surface density of M33 at 12 kpc, 2.6×10^{-3} g/cm^2. The magnitude of the tidal effect of M31 on M33 should therefore be just about twice the tidal effect of the Magellanic Clouds on the Milky Way. However, it has been shown (Burke 1957; Kerr 1957; Avner and King 1967; Hunter and Toomre 1968) that the tidal effects of the Magellanic Clouds on the Milky Way are insufficient to account for

the observed hatbrim unless they were at one time significantly closer than at present. In order to understand the observed distortion of the isovels in M33 as a tidally induced hatbrim, one would have to postulate a close approach to M31.

If one interprets the anomalous radial velocities in the wings of M33 as motion perpendicular to the plane rather than expansion, one finds velocities with the magnitudes listed in the sixth line of Table 12. Calculation of the surface density from the rotation curve, together with the assumption that the galaxy is an infinite sheet with uniform surface density, lead to the accelerations K_z listed in the seventh line of the table. If the matter in the wings of M33 is currently in the plane and moving with the indicated velocity perpendicular to the plane, then it will ultimately reach the heights listed in the last line of the table. Since these heights are so large as to make the assumption of an infinite sheet a poor approximation to the actual aspect of the galaxy, an alternate calculation was made in which the galaxy was represented as a point source of $2.3 \times 10^{10}\ M_{\odot}$, the mass of M33 contained within a cylinder of 60' radius. The z component of the gravitational acceleration computed in this fashion was always at least 30% smaller than that calculated for the infinite sheet. Consequently, the listed heights cannot be reduced by more than a third, even if one assumes that the correct value for the acceleration is the sum of the two accelerations calculated.

The assumptions of increased space density or increased thickness of the hydrogen layer are in effect similar to each other, but different from the assumption of a warped layer, in that they both imply a physical piling-up of the gas at certain position angles in the galaxy (like

physical arms or density waves). While explaining the integrated H I aspect of the wings, neither model explains the observed velocity anomalies without additional assumptions. If one removes the restriction of having the wings physically connected to the plane of M33, one has a model of two self-contained masses of neutral hydrogen: companions in arbitrary orbits around the galaxy.

Two checks can be made on whether it is possible for the wings to exist as stable entities. First is to calculate the tidal limit on their size imposed by M33 itself. According to King (1962),

$$r_t = R(M/2M_g)^{1/3} \quad . \tag{4.19}$$

For R we use the characteristic distances in Table 12, for M the masses of the wings, and for M_g $2.3 \times 10^{10}\ M_\odot$, the mass of M33 within a limiting radius of 60'. These figures yield tidal limiting radii r_t = 9!1 and 5!7, to be compared with observed radii r_ℓ = 7' and 5!3 for the np and sf wings, respectively. Second is to apply the virial theorem in its simplest form,

$$MV^2 = GM^2/r_\ell \quad . \tag{4.20}$$

An estimated half width of 30 km/sec for velocity profiles in the wings yields an r.m.s. space velocity of 22 km/sec. With this velocity and the masses and radii quoted above, the left side of the equation assumes a value of 1×10^{54} ergs for the np wing and 5×10^{53} ergs for the sf wing, while the right side assumes values of 6×10^{53} ergs and 2×10^{53} ergs, respectively. These results are consistent with the stability of the wings, to the accuracy of the data.

The presence of two neutral hydrogen companions relatively near to the main body of M33 could produce distortions in the outer parts of the galactic plane which might explain the smaller velocity anomalies at other position angles in Figures 16 and 17. Unfortunately there are too many unknown parameters to allow a quantitative evaluation of this model.

CHAPTER V: SUMMARY

Messier 33 is a particularly interesting object for study in the 21-cm spectral line of neutral atomic hydrogen. As the late-type spiral galaxy of largest angular size, it is the prototype of the most numerous class of external galaxies available for this type of study. In addition, it provides together with M31 a pair of galaxies which are probably quite similar to our own, and such that many parameters of our own galaxy may be interpolated between their values for the corresponding parameters.

Table 13 summarizes the properties of M33. For comparison with several of the quantities in the table, one may use the following mean values derived for Scd systems (Roberts 1968b): $\langle M_{HI}/L_O \rangle = 0.48$ (ten systems), $\langle M_{HI}/M_t \rangle = 0.10$ (eight systems), and $\langle M_t/L_O \rangle = 6.7$ (eight systems). Individual values for each of these ratios show a large scatter about the mean. The distribution of neutral hydrogen is much larger than the distributions of optical and radio continuum emission, luminous stars, and H II regions. In addition, it is ring-shaped (i.e., with a central minimum), while the other distributions are all centrally peaked. The distribution of total mass, though centrally peaked, covers an even larger area than the neutral hydrogen.

From the results of this study one can conclude that the first approximation to the galaxy of an axisymmetric thin disk in circular rotation is a good one, although it fails in detail (and the more detail one sees in a galaxy, the more departures from circular symmetry one can find). The asymmetry found in the rotation curves for the two halves of the major axis of M33 has its parallels in the rotation-curve asymmetries in M31 (Roberts 1966) and the Milky Way (Kerr 1962).

TABLE 13

SUMMARY OF THE PROPERTIES OF MESSIER 33

Position (Shapley and Ames 1932)	α δ (1950)	$1^h\ 31.^m1$ +30° 24'
Distance (Sandage 1962)	$(m-M)_o$ D	24.3 mag 720 kpc
Apparent distance moduli (Sandage 1962) (de Vaucouleurs 1966)	$m_{pg}-M_{pg}$ m_B-M_B	24.68 mag 24.6 mag
Optical diameter (Holmberg 1950) (0.1 of smeared peak)		83'x53' 50'x34'
H I diameter (0.1 of peak)		93'x56'
Inclination	i	55°
Systemic radial velocity, heliocentric	S	-180 km/sec
Structural type (van den Bergh 1960) (de Vaucouleurs 1961a)		Sc II-III SA(s)cd
Parameters of H I distribution:		
ring radius	r_o	18'
ring width	σ_H	10'
disk radius	r_D	35'
maximum relative surface density, ring/disk	H_o/H_D	0.66
Maximum H I surface density, corrected to face-on view	N_{HI}	1.1×10^{21} cm^{-2}
Mass of neutral atomic hydrogen	M_{HI}	1.6×10^9 $M_\odot$
Mean rotation-curve parameters:		
peak velocity, line of sight component	V_m	84 km/sec
peak circular velocity	V_m cosec i	103 km/sec
radius at peak	R_m	30'
shape parameter	n	1.0
velocity dispersion	σ_v	13 km/sec
Total mass, extrapolated within cylinder of radius 60'	M_t M_{60}	4.9×10^{10} $M_\odot$ 2.3×10^{10} $M_\odot$
Photographic luminosity corrected for inclination and galactic extinction	L_0	4.7×10^9 $L_\odot$
Color index corrected for inclination and galactic reddening	C_0	0.29 mag
Fraction of mass as neutral atomic hydrogen	M_{HI}/M_{60} M_{HI}/M_t	0.070 0.033
Mass-to-light ratio	M_{60}/L_0 M_t/L_0 M_{HI}/L_0	4.9 $M_\odot/L_\odot$ 10.4 $M_\odot/L_\odot$ 0.34 $M_\odot/L_\odot$

Asymmetries are also found in the distribution of neutral hydrogen (see Fig. 4). An interesting detail is the detection of an H I concentration apparently associated with the giant H II region NGC 604. This is analogous to the H I - H II complexes in the Large Magellanic Cloud (McGee and Milton 1966), and to the Orion aggregation in our galaxy (Gordon 1969). On a larger scale are the offsets of the centers of the distributions of H I, H II regions, and O stars from the optical center of the galaxy. The offsets (several minutes of arc or several hundred parsecs in size) are not accompanied by large velocity anomalies near the center of M33--there is no evidence for an explosion, as in M82, or for an analog of the 4-kpc expanding arm in our galaxy. The perturbation of the distribution of extreme Population I objects with respect to the older constituents of M33 seems, therefore, likely to be quiet and evolutionary rather than cataclysmic in origin.

The most striking departures from circular symmetry in both the hydrogen distribution and velocity field of M33 are the wings (see Figs. 3 and 16). Similar distortions of the radial-velocity loci have been found for NGC 300 (Shobbrook and Robinson 1967) and NGC 5236 (Lewis 1968). In the former study, several models were proposed, but the resolution of the data was insufficient to allow a choice among them. In the latter study, no attempt was made to reconcile the resulting picture of the kinematics with the optical appearance of the galaxy, and the fact that the locus of the systemic velocity was aligned with the optical minor axis rather than perpendicular to the line joining the velocity extrema was interpreted as an indication of expansion in the main body of the galaxy. In the case of M33, at least, it would be unwarranted to ignore the kinematical studies at optical wavelengths which are inconsistent

with such a picture--particularly since there is good agreement between these studies and the present data for the main body of the galaxy. However, attempts to explain the wings as distortions of the plane of M33 like the "hatbrim" of the Milky Way lead to extreme values of several parameters, notably the maximum height of the wings above the galactic plane. Since tidal forces are too weak to explain the "hatbrim", they fail by a larger factor to account for the wings. The present observations are consistent with a picture of the wings as stable, gaseous companions of M33, containing $\sim 10^8 M_\odot$ of neutral hydrogen, in orbits which are noncircular and/or inclined to the galactic plane. Hydrogen companions have previously been found for M31 (Burke, Turner, and Tuve 1964a) and NGC 925 (Höglund and Roberts 1965). It is also possible to interpret the high-velocity clouds found during surveys of the hydrogen in our galaxy (Hulsbosch and Raimond 1966) as similar companions of the Milky Way (Kerr 1968).

A search was made along a line connecting the centers of M31 and M33 for a possible bridge of neutral atomic hydrogen linking the two galaxies. The upper limit on the surface density of hydrogen in the region between the galaxies is $N_{HI} \leq 5 \times 10^{14}$ atoms/cm^2. This limit is 1/4 the observed density in the bridge between NGC 4631 and NGC 4656 (Roberts 1968a) and 1/6 the observed density between the Magellanic Clouds (Hindman et al. 1963).

The model-fitting technique used in this study is a powerful tool for studying the kinematics of galaxies. With a large galaxy like M33, it yields a detailed picture. In addition, it can extract parameters for galaxies which are not much larger than the half-power beamwidth of

the telescope (Roberts 1968a; Gordon, Remage, and Roberts 1968). The present study of M33 is the most detailed, overall, 21-cm study of this type of galaxy possible with presently available instruments. Other galaxies which allow more detailed overall study are M31, because of its greater size, and the Magellanic Clouds, because of their greater proximity. Examples of further surveys of M33 which should be undertaken in the near future are (1) surface photometry with an Hα interference filter to provide a less biased view of the distribution of ionized hydrogen than can be obtained from the present catalogs of emission regions, and (2) extension of the star counts to fainter limiting magnitudes and to a second color in order to yield a better picture of the upper end of the luminosity function and stellar evolution.

BIBLIOGRAPHY

Alexander, S., 1852, A. J., 2, 95.

Allêr, L. H., 1942a, Ap. J., 95, 48.

————, 1942b, Ap. J., 95, 52.

————, 1954, Astrophysics: Nuclear Transformations, Stellar Interiors, and Nebulae (New York: Ronald Press), p. 23.

————, 1956, Gaseous Nebulae (New York: John Wiley and Sons).

Aller, L. H., Czyzak, S. J., and Walker, M. F., 1968, Ap. J., 151, 491.

Aller, L. H., and Faulkner, D. J., 1962, Pub. A.S.P., 74, 219.

Avner, E. S., and King, I. R., 1967, A. J., 72, 650.

Balister, M., 1968, N.R.A.O. Electronics Div. Int. Rep., No. 70.

Bergh, S. van den, 1960, Ap. J., 131, 215.

Blaauw, A., 1963, in Stars and Stellar Systems, Vol. 3: Basic Astronomical Data, ed. K. Aa. Strand (Chicago: Univ. of Chicago Press), p. 383.

Bottlinger, K. F., 1933, Veröff. Berlin-Babelsberg, 10, No. 2.

Brandt, J. C., 1960, Ap. J., 131, 293.

————, 1965, M.N.R.A.S., 129, 309.

Brandt, J. C., and Scheer, L. S., 1965, A. J., 70, 471.

Brown, R. H., and Hazard, C., 1959, M.N.R.A.S., 119, 297.

————, 1961, M.N.R.A.S., 122, 479.

Burke, B. F., 1957, A. J., 62, 90.

Burke, B. F., Turner, K. C., and Tuve, M. A., 1963, Carnegie Inst. Wash. Year Book, 62, 289.

————, 1964a, Carnegie Inst. Wash. Year Book, 63, 341.

————, 1964b, I.A.U. Symp. No. 20: The Galaxy and the Magellanic Clouds, ed. F. J. Kerr and A. W. Rodgers (Canberra: Australian Acad. Sci.), p. 99.

Carranza, G., Courtès, G., Georgelin, Y., Monnet, G., and Pourcelot, A., 1968, Ann. d'Ap., 31, 63.

Courtès, G., and Cruvellier, P., 1961, Comptes Rendus, 253, 218.

————, 1965, Ann. d'Ap., 28, 683.

Curtis, H. D., 1917, Pub. A.S.P., 29, 180.

————, 1918, Pub. Lick Obs., 13, 57.

Danver, C. G., 1942, Lund Obs. Ann., 10.

Davies, R. D., I.A.U. Symp. No. 31: Radio Astronomy and the Galactic System, ed. H. van Woerden (London: Academic Press), p. 199.

Davis, M. M., and Hagstrom, M., 1968, N.R.A.O. Electronics Div. Int. Rep., No. 68.

DeJong, M. L., 1965, Ap. J., 142, 1333.

————, 1967, Ap. J., 150, 1.

Dieter, N. H., 1957, Pub. A.S.P., 69, 356.

————, 1962, A. J., 67, 217.

Dreyer, J.L.E., 1904, Proc. Roy. Irish Acad., 25A, 3.

Duncan, J. C., 1922, Pub. A.S.P., 34, 290.

Gingerich, O., 1960, Sky and Tel., 19, 207.

Gordon, C. P., 1969, private communication.

Gordon, K. J., 1968, A. J., 73, S14.

Gordon, K. J., Remage, N. H., and Roberts, M. S., 1968, Ap. J., 154, 845.

Haro, G., 1950, A. J., 55, 66.

Heeschen, D. S., 1961, Pub. N.R.A.O., 1, 129.

Heeschen, D. S., and Wade, C. M., 1964, A. J., 69, 277.

Hiltner, W. A., 1960, Ap. J., 131, 163.

Hindman, J. V., Kerr, F. J., and McGee, R. X., 1963, Austral. J. Phys., 16, 570.

Höglund, B., and Roberts, M. S., 1965, Ap. J., 142, 1366.

Holmberg, E., 1950, Lund. Obs. Medd., Ser. II, No. 128.

————, 1952, Lund Obs. Medd., Ser. I, No. 180.

————, 1958, Lund Obs. Medd., Ser. II, No. 136.

Howard, W. E., III, 1961, A. J., 66, 521.

Hubble, E. P., 1925, Pop. Astr., 33, 252.

————, 1926, Ap. J., 63, 236.

————, 1932, Ap. J., 76, 44.

————, 1935, Ap. J., 81, 334.

————, 1936, The Realm of the Nebulae (New Haven, Conn.: Yale Univ. Press).

————, 1943, Ap. J., 97, 112.

Hubble, E. P., and Sandage, A. R., 1953, Ap. J., 118, 353.

Hulsbosch, A.N.M., and Raimond, E., 1966, B.A.N., 18, 413.

Hulst, H. C. van de, Raimond, E., and Woerden, H. van, 1957, B.A.N., 14, 1.

Humason, M. L., Mayall, N. U., and Sandage, A. R., 1956, A. J., 61, 97.

Hunter, C., and Toomre, A., 1968, A. J., 73, S100.

Johnson, H. L., Hoag, A. A., Iriarte, B., Mitchell, R. I., and Hallam, K. L., 1961, Lowell Obs. Bull., 5, 133 (No. 113).

Johnson, H. L., and Morgan, W. W., 1953, Ap. J., 117, 313.

Keeler, J. E., 1908, Pub. Lick Obs., 8.

Kerr, F. J., 1957, A. J., 62, 93.

————, 1962, M.N.R.A.S., 123, 327.

————, 1968, A. J., 73, S102.

————, 1969, Ann. Rev. Astr. Ap., 7 (in press).

Kerr, F. J., and Vaucouleurs, G. de, 1956, Austral. J. Phys., 9, 90.

Kerr, F. J., and Westerhout, G., 1965, in Stars and Stellar Systems, Vol. 5: Galactic Structure, ed. A. Blaauw and M. Schmidt (Chicago: Univ. of Chicago Press), p. 167.

King, I. R., 1962, A. J., 67, 471.

Kron, G. E., and Mayall, N. U., 1960, A. J., 65, 581.

Kurchatov, V. N., and Sytsko, G. A., 1965, Sov. Astr.—AJ, 9, 421. (A. Zh., 42, 531).

Leslie, P.R.R., 1960, Observatory, 80, 216.

Lewis, B. M., 1968, Proc. A. S. Australia, 1, 104.

Lindblad, B., 1948, Stockholm Obs. Ann., 15, No. 4.

Lindblad, B., and Brahde, R., 1946, Ap. J., 104, 211.

Lohmann, W., 1954, Zs. f. Ap., 35, 159.

Lundmark, K., 1921, Pub. A.S.P., 33, 324.

————, 1926, Ap. J., 63, 67.

————, 1927, Medd. Astr. Obs. Upsala, No. 30.

Maanen, A. van, 1916, Proc. Nat. Acad. Sci., 2, 386.

————, 1923, Ap. J., 57, 264.

————, 1935, Ap. J., 81, 336.

Mathis, J. S., 1962, Ap. J., 136, 374.

Mayall, N. U., 1939, Lick Obs. Bull., 19, 33 (No. 497).

————, 1951, Pub. Obs. Univ. Mich., 10, 19.

Mayall, N. U., and Aller, L. H., 1939, Pub. A.S.P., 51, 112.

————, 1940, Pub. A.S.P., 52, 278.

————, 1942, Ap. J., 95, 5.

McClure, R. D., and Bergh, S. van den, 1968, A. J., 73, 313.

McGee, R. X., and Milton, J. A., 1966, Austral. J. Phys., 19, 343.

McVittie, G. C., 1965, General Relativity and Cosmology, 2d ed. (London: Chapman and Hall), pp. 197-204.

Meng, S. Y., 1968, private communication.

Meng, S. Y., and Kraus, J. D., 1966, A. J., 71, 170.

Morgan, W. W., 1958, Pub. A.S.P., 70, 364.

————, 1959, Pub. A.S.P., 71, 394.

Oort, J. H., 1965, in Stars and Stellar Systems, Vol. 5: Galactic Structure, ed. A. Blaauw and M. Schmidt (Chicago: Univ. of Chicago Press), p. 455.

Pahlen, E. van der, 1911, A. N., 188, 249.

Patterson, F. S., 1940, Harvard Bull., No. 914, 9.

Pease, F. G., 1915, Pub. A.S.P., 27, 239.

————, 1916, Pub. A.S.P., 28, 33.

Pickering, E. C., 1917, Harvard Bull., No. 641.

Pilkington, J.D.H., and Scott, P. F., 1965, Mem. R.A.S., 69, 183.

Rhijn, P. J. van, 1936, Groningen Pub., No. 47.

Ritchey, G. W., 1917, Pub. A.S.P., 29, 210.

Roberts, I., 1893, A Selection of Photographs of Stars, Star-Clusters and Nebulae (London: The Universal Press).

————, 1899, Photographs of Stars, Star-Clusters and Nebulae. Vol. II (London: The Universal Press).

Roberts, M. S., 1965, Ap. J., 142, 148.

————, 1966, Ap. J., 144, 639.

————, 1967, I.A.U. Symp. No. 31: Radio Astronomy and the Galactic System, ed. H. van Woerden (London: Academic Press), p. 189.

————, 1968a, Ap. J., 151, 117.

————, 1968b, in Stars and Stellar Systems, Vol. 9: Galaxies and the Universe, ed. A. and M. Sandage (Chicago: Univ. of Chicago Press), chap. xi (preprint).

Rosse, W. Parsons, Earl of, 1850, Phil. Trans., 140, 499.

Sandage, A. R., 1958, Ric. Astr., Spec. Vatican, 5, 75.

Sandage, A. R., 1962, I.A.U. Symp. No. 15: Problems of Extra-Galactic Research, ed. G. C. McVittie (New York: Macmillan), p. 359.

Scheiner, J., 1899, Ap. J., 9, 149.

Schwarzschild, M., 1954, A. J., 59, 273.

Sěrsic, J. L., 1959a, unpublished, communicated to me by A. R. Sandage.

————, 1959b, Observatory, 79, 54.

————, 1960, Zs. f. Ap., 50, 168.

Seyfert, C. K., 1940, Ap. J., 91, 528.

Shajn, G. A., 1954, Isv. Crimean Ap. Obs., 11, 3.

Shajn, G. A., and Haze, V. F., 1952, Isv. Crimean Ap. Obs., 9, 13.

————, 1953, A. Zh., 30, 481.

Shalloway, A. M., 1964, NEREM Record, 6, 98.

Shane, W. W., and Smith, G.P.B., 1966, B.A.N., 18, 263.

Shapley, H., and Ames, A., 1932, Harvard Ann., 88, 41.

Shobbrook, R. R., and Robinson, B. J., 1967, Austral. J. Phys., 20, 131.

Slipher, V. M., 1914, Lowell Obs. Bull., 2, 56 (No. 58).

————, 1915, Pop. Astr., 23, 21.

Stebbins, J., and Kron, G. E., 1957, Ap. J., 126, 266.

Stebbins, J., and Whitford, A. E., 1937, Ap. J., 86, 247.

————, 1948, Ap. J., 108, 413.

————, 1952, Ap. J., 115, 284.

Strauss, F., 1968, Ann. Rep. Dir. Dept. Terrestrial Magnetism, p. 61.

Takase, B., 1957, Pub. A.S. Japan, 9, 16.

Takase, B., and Kinoshita, H., 1967, Pub. A.S. Japan, 19, 409.

Tammann, G. A., and Sandage, A. R., 1968, Ap. J., 151, 825.

Tifft, W. G., 1961, A. J., 66, 390.

Turner, K. C., 1968, discussion following paper by K. J. Gordon at 127th A.A.S. meeting

Vaucouleurs, G. de, 1958, Ap. J., 127, 487.

————, 1959, Ap. J., 130, 728.

————, 1961a, Ap. J. Suppl., 5, 233 (No. 48).

————, 1961b, Year Book Amer. Phil. Soc., p. 268.

————, 1966, in Stars and Stellar Systems, Vol. 9: Galaxies and the Universe, ed. A. and M. Sandage (Chicago: Univ. of Chicago Press), chap. xvii (preprint).

————, 1968, private communication.

Vaucouleurs, G. de, and Ables, H., 1965, Pub. A.S.P., 77, 272.

Venugopal, V. R., 1963, Pub. A.S.P., 75, 404.

Volders, L.M.J.S., 1959, B.A.N., 14, 323.

Vorontsov-Velyaminov, B. A., 1955, A. Zh., 32, 401.

————, 1956a, A. Zh., 33, 14.

————, 1956b, A. Zh., 33, 205.

Vorontsov-Velyaminov, B. A., and Arkhipova, V. P., 1964, Morphological Catalogue of Galaxies. Part II (Moscow: Moscow Univ. Press), p. 117.

Voshakidze, M. A., 1955, Bull. Abastumani Ap. Obs., No. 18, 15.

Walker, M. F., 1964, A. J., 69, 744.

————, 1967, Pub. A.S.P., 79, 119.

Weinreb, S., 1963, MIT Res. Lab. Electronics Tech. Rep., No. 412.

Whitford, A. E., 1936, Ap. J., 83, 424.

————, 1962, A. J., 67, 640.

————, 1963, A. J., 68, 637.

Wolf, M., 1914, Vjs. astr. Ges., 49, 151.

Wolf, M., and Ernst, E., 1913, Veröff. Strnw. Heidelberg, 6, 115.

Wood, D. B., 1966, Ap. J., 145, 36.

Wyse, A. B., and Mayall, N. U., 1941, Pub. A.S.P., 53, 269.

————, 1942, Ap. J., 95, 24.